

**QUANTUM KINETICS AND THE ZENO ANSATZ:
STERILE NEUTRINO DARK MATTER IN THE EARLY UNIVERSE**

A Thesis
Presented to the
Faculty of
San Diego State University

In Partial Fulfillment
of the Requirements for the Degree
Master of Science
in
Physics

by
Olexiy V. Dvornikov
Summer 2017

ProQuest Number: 10636584

All rights reserved

INFORMATION TO ALL USERS

The quality of this reproduction is dependent upon the quality of the copy submitted.

In the unlikely event that the author did not send a complete manuscript and there are missing pages, these will be noted. Also, if material had to be removed, a note will indicate the deletion.



ProQuest 10636584

Published by ProQuest LLC (2017). Copyright of the Dissertation is held by the Author.

All rights reserved.

This work is protected against unauthorized copying under Title 17, United States Code
Microform Edition © ProQuest LLC.

ProQuest LLC.
789 East Eisenhower Parkway
P.O. Box 1346
Ann Arbor, MI 48106 – 1346

SAN DIEGO STATE UNIVERSITY

The Undersigned Faculty Committee Approves the


Thesis of Olexiy V. Dvornikov:

Quantum Kinetics and the Zeno Ansatz:

Sterile Neutrino Dark Matter in the Early Universe



Fridolin Weber, Chair
Department of Physics



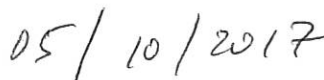
Arlette Baljon
Department of Physics



Robert Quimby
Department of Astronomy



Chad Kishimoto
Department of Physics, University of San Diego



Approval Date

Copyright © 2017
by
Olexiy V. Dvornikov

DEDICATION

To my mom,
for all of her love and support

There are only two questions worth asking.
Why are we here? And what should we do about it while we are?

– John Lloyd

ABSTRACT OF THE THESIS

Quantum Kinetics and the Zeno Ansatz:
Sterile Neutrino Dark Matter in the Early Universe

by
Olexiy V. Dvornikov
Master of Science in Physics
San Diego State University, 2017

We solved the quantum kinetic equations for the evolution of neutrino states in the early universe. Starting at high temperatures, we evolve neutrino states to observe the resonant conversion of active-to-sterile neutrinos in a lepton asymmetric (more neutrinos than anti-neutrinos) universe. We find that at high temperatures, the high neutrino scattering and oscillation rates enforce a local equilibrium that balances the growth of coherence at the oscillation rate and the damping of coherence through scattering. This equilibrium, which we call a “quantum kinetic equilibrium,” appears to approximately hold throughout the neutrino evolution, from the initial conditions through resonances that may be non adiabatic. Using this quantum kinetic equilibrium informs a proper choice of the initial conditions of the neutrino state and the relaxation process that occurs to this equilibrium when the initial conditions (as are typically chosen in the literature) are not coincident with the equilibrium values. We also discuss how to use this equilibrium to reduce the computational expense of solving the full quantum kinetic equations for neutrino states evolving in the early universe.

TABLE OF CONTENTS

	PAGE
ABSTRACT	vi
LIST OF FIGURES	viii
ACKNOWLEDGMENTS	xi
CHAPTER	
1 Introduction	1
1.1 History	1
1.2 The 3.5 keV Line and Sterile Neutrinos.....	2
1.3 Neutrino Cosmology	3
1.4 Neutrino Decoupling	6
1.5 Big Bang Nucleosynthesis	7
1.6 Vacuum Mixing	8
1.7 In Medium Mixing	10
1.8 Adiabatic In Medium Mixing.....	12
1.9 Quantum Kinetic Equations	13
1.10 Motivation of the Quantum Kinetic Equations	17
1.11 Zeno Equations	19
2 My Research	25
2.1 Numerical Methods	25
2.2 Solutions to the QKEs	26
2.3 Quantum Kinetic Equilibrium	30
2.4 The Geometry of the QKEs at Resonances	34
2.5 Initial Conditions and “Ringing”	38
3 Conclusion.....	43
BIBLIOGRAPHY	45

LIST OF FIGURES

	PAGE
Figure 1.1. Sterile neutrino dark matter parameter space adopted with permission from [32]. The shaded regions are consistent with the x-ray signal at 1, 2, and 3σ . The blue contours come from a stacked spectrum of 73 clusters obtained with the MOS detectors on XMM Netwon. Statistically consistent signals are found in the Perseus spectrum and M31. The lines show constraints at the 90% level from <i>Chandra</i> observations of M31, stacked dwarf galaxies, and Suzaku observations of Perseus. The stars mark the models studied by [32]	3
Figure 1.2. Survival probability P_{ν_μ} vs. [meters/MeV] for $\nu_\mu \leftrightarrow \nu_\tau$ oscillations for $\delta m^2 = 2.4 * 10^{-3}$ eV and $\sin^2 2\theta = 0.92$	10
Figure 1.3. Schematic of P precessing around V for the case of a coherent evolution.	19
Figure 1.4. A sterile neutrino spectrum at $T = 50$ MeV as a function of scaled momentum x . This evolution is for $m_s = 64$ keV, $\sin^2 \theta = 10^{-10}$, and $L_0 = 1.1 * 10^{-3}$	21
Figure 1.5. A phase space distribution at $T = 10$ MeV for a sterile neutrino mass of $m_s = 7.1$ keV. The mixing angle $\sin^2 2\theta$ is varied and shown in different colors. This figure is adopted with permission from [32] and assumes 2×2 mixing between ν_s and ν_μ . The y-axis is multiplied by a massless Fermi-Dirac distribution with degeneracy $g = 0.003$	22
Figure 1.6. The evolution of the lepton number (initially $L_0 = 1.1 \times 10^{-3}$) for $m_s = 64$ keV and $\sin^2 2\theta = 10^{-10}$	23
Figure 1.7. Percent difference between the sterile neutrino conversion rate df/dT for scaled momentum $x = 1$ between the Zeno equations and the QKEs. Both systems of equations are for an evolving lepton number (initially $L_0 = 1.1 \times 10^{-3}$) and $m_s = 64$ keV and $\sin^2 2\theta = 10^{-10}$. The jagged behavior is due to the interpolation method used compare the two solutions.	24
Figure 2.1. Solutions to the QKEs for a constant lepton number $L = 1.1 \times 10^{-3}$ ($m_s = 64$ keV, $\sin^2 2\theta = 10^{-10}$). The top two panels show $10^4 P_x$ and $-10^4 P_y$ vs. T , the middle two panels show P_0 and P_z vs. T , and the bottom panel shows the sterile neutrino conversion rate df/dT for $x = 1$	28
Figure 2.2. Solutions to the QKEs for an evolving lepton number L . Initially, $L_0 = 1.1 \times 10^{-3}$. As for the constant lepton number case, $m_s = 64$ keV and $\sin^2 2\theta = 10^{-10}$. The top two panels show $10^4 P_x$ and $-10^4 P_y$ vs. T and the middle two panels show P_0 and P_z vs. T . The bottom left panel shows the evolution of L and the bottom right panel shows the sterile neutrino conversion rate df/dT for $x = 1$	29

- Figure 2.3. The oscillation frequency ω (blue) and the scattering frequency Γ (red) in units of inverse MeV vs. temperature. The time increases to the left. 31
- Figure 2.4. $(1 - Abs(E/F))$ vs. T for a constant lepton number, where E corresponds to the equilibrium values of P_x (blue) and P_y (red) and F to the full values. The equilibrium P_x and P_y depend on P_0 and P_z , which we took from the full solutions to the QKEs. 31
- Figure 2.5. $(1 - Abs(E/F))$ vs. T for a constant lepton number, where E corresponds to the equilibrium solutions and F to the full solutions. The comparison is blue for P_x and red for P_y (top box), and magenta for P_0 and green for P_z (bottom box). 33
- Figure 2.6. The top left panel is $\cos \theta$ where θ is the angle between \mathbf{V} and \mathbf{P} . The top right panel is $\sin^2 \theta$. The bottom left panel is $\sin^2 \theta_M$ where θ_M is the in medium mixing angle. The bottom right panel is the difference of $\sin^2 \theta_M$ and $\sin^2 \theta$. These figures are for a constant lepton number. 36
- Figure 2.7. Constant lepton number evolution of the unit projections of \mathbf{P} (top left), \mathbf{V} (top right), and $\mathbf{V} \times \mathbf{P}$ (bottom) through a resonance. Points 1,2, and 3 correspond to progressively decreasing temperatures of $T = 624.385$ MeV, $T = 624.377$ MeV, and $T = 624.369$ MeV, or alternatively, increasing time. The resonance happens at Point 2. 37
- Figure 2.8. Unit projections of \mathbf{P} (top left), \mathbf{V} (top right), and $\mathbf{V} \times \mathbf{P}$ (bottom) through a resonance for the case of an evolving lepton number. Just as in Figure 2.7 the temperature decreases as the arc swings from right to left in the top left and the bottom panels. In the top right panel, the temperature decreases as the arc swings from 1 to -1. The first point corresponds to $T = 953.606$ MeV; the last to $T = 953.600$ MeV. Due to a changing lepton number, the resonance (the point at $x = 0$) happens at a different temperature than in Figure 2.7 38
- Figure 2.9. Ringing of P_x for a span of 10 eV after 2 GeV. The x axis is $(2 \text{ GeV} - T)$. The time increases to the right. The oscillation frequency is $\omega = |\mathbf{V}| = 2.1 \times 10^{-4} \text{ MeV}^{-1}$ and the damping frequency is $\xi = \mathcal{D} = 2.8 \times 10^{-6} \text{ MeV}^{-1}$. This evolution is for a constant lepton number. 40
- Figure 2.10. The oscillation frequency ω (red) and the damping frequency ξ (blue) in units of $1/\text{MeV}$ vs. temperature (MeV) for a constant lepton number. We chose the bolded points to test the underdamped oscillator model. Figure 2.9 shows the point corresponding to $T = 2000$ MeV, where $\omega = 2.1 \times 10^{-4} \text{ MeV}^{-1}$ and $\xi = \mathcal{D} = 2.8 \times 10^{-6} \text{ MeV}^{-1}$ 40
- Figure 2.11. Two initial values of P_x relaxing to the same equilibrium point with the same oscillation frequency ω and damping frequency ξ . The plot shows a span of 20 eV after 2 GeV. The x axis is $(2 \text{ GeV} - T)$. The temperature decreases to the right and the time increases to the right. 41

Figure 2.12. P_x for different step sizes. The blue lines corresponds to $dT = 3.8 \times 10^{-2}$ eV and the red line corresponds to $dT = 7.5 \times 10^{-2}$ eV. The plot shows a span of 7 eV after 1.5 GeV. The x axis is $(1.5 \text{ GeV} - T)$. The temperature decreases to the right and the time increases to the right. Each step size settles to the same equilibrium. 42

ACKNOWLEDGMENTS

I would like to thank Dr. Kishimoto and Dr. Weber for the time that they invested in me and for helping me dive into research in cosmology. Also, I would like to thank Dr. Baljon and Dr. Quimby for joining my committee.

CHAPTER 1

INTRODUCTION

Neutrinos are ubiquitous. About 60 billion solar neutrinos cross every cm^2 of our body per second. Exploding supernovae release 99% of their gravitational binding energy in neutrinos. And even in cosmic voids, the average number density of cosmological neutrinos is $n \sim 336 \text{ cm}^{-3}$ [33, pp. 334]. We truly live immersed in neutrinos, and yet we scarcely affected by them. Why?

Neutrinos are by far the lightest fermions and interact unbelievably weakly compared to the other particles. For instance, neutrinos of $E \sim 1 \text{ MeV}$ have a cross section of $\sigma \sim 10^{-44} \text{ cm}^2$. This means that only 1 in 10^{11} streaming through the Earth will interact with an atom. In other words, we need humongous detectors for appreciable detection rates.

And if neutrinos were not odd enough, two decades ago physicists discovered another truly mind-boggling property [6, 18]. Neutrinos exist as superpositions of masses. And since different masses evolve differently, this means that neutrino flavors can *change*.

1.1 HISTORY

The motivation for neutrinos came from the study of radioactive decays at the turn of the last century. In 1914, James Chadwick showed that β decays, unlike the α and γ decays, had a continuous spectrum [12]. An example of this is the decay of a free neutron into a proton and an electron. One expects the e^- to have a defined energy, but experimentalists found a continuous spectrum. To preserve the tenet of energy conservation, Wolfgang Pauli speculated that a new particle, the neutrino, must also be emitted [29]. It must be neutral to conserve charge, very light to obey energy conservation, and have a spin of $1/2$ for statistical reasons. Also, to match the observed rates of e^\pm emitted in β decays, the neutrino must interact extremely weakly. In fact, neutrinos interact so feebly that they were not detected until 1956 [13]. So far, we have found three species, the electron neutrino ν_e , the muon neutrino ν_μ , and the tau neutrino ν_τ , and the Standard Model assumes that the neutrinos are massless. But, even in 1957, Pontecorvo thought of neutrinos changing flavors [30]. And in 1998, T. Kajita of the Super-K Collaboration presented data indicating a disappearance of muon neutrinos spewed out of cosmic ray interactions with the atmosphere [18]. Additionally in 2001, A. McDonald of the Sudbury Collaboration showed evidence for the flavor conversions of neutrinos emanating from the sun [6]. These discoveries of massive and oscillating neutrinos, force us to rethink what we know about particle physics and maybe even

dark matter. And to add to the madness, recent experiments offer tantalizing clues to the existence of yet another neutrino.

1.2 THE 3.5 KEV LINE AND STERILE NEUTRINOS

Physicists have searched for and failed to find interactions between dark matter and baryonic matter [9]. Yet recently, A. Boyarsky and colleagues [10] have spotted an anomalous x-ray line in Andromeda and the Perseus cluster. These x-rays could originate from decaying dark matter; in particular, keV range sterile neutrinos. A sterile neutrino is theorized to only interact gravitationally with normal matter and via oscillations with other neutrinos. Unlike, the other three neutrino flavors, the sterile neutrino is right-handed, meaning that its spin and momentum are anti-parallel. Analogous to regular neutrinos, a sterile neutrino has no definitive mass, but rather exists as a superposition of masses. Therefore, it oscillates and can decay weakly into an x-ray and a lighter neutrino.

Massive neutrinos are an ideal explanation for dark matter. Dark matter particles with large velocity dispersions, or Hot Dark Matter, contradict the observations of the evolution of cosmological perturbations, and for the past thirty years researchers have focused their attention on Cold Dark Matter and Warm Dark Matter.

The virial speed of dark matter demands that such a sterile neutrino is nonrelativistic and massive and since it decays into a light neutrino and a massless photon both have an energy of $m_s/2$, where m_s is the mass of the sterile neutrino. This decay, if real, has a mean lifetime longer than the age of the universe but a cluster of galaxies has more than enough dark matter for us to observe it.

To claim that the anomalous x-ray emission is due to decaying dark matter we must be absolutely sure that nothing else could be the source. After all, hot plasma is ubiquitous in galaxy clusters and it has many atomic transitions. Fortunately, we understand these transitions and none of them match the recently observed line at 3.5 keV. Also, Andromeda does not have hot enough gas for such emission lines yet it streams x-rays [11]. Furthermore, the line appears brighter in systems with more dark matter, as expected if decaying dark matter is the culprit. However, this observation is still heavily disputed.

The hints are tantalizing but only future experiments can settle the debate. Astrophysicists hoped that the Hitomi satellite launched in 2016 would point us in the right direction. It had a spectral resolution 20 times better than the previous missions and could resolve the width and flux of the line. A broad line would signify Doppler broadening of dark matter particles and a narrow line would point to a normal atomic transition which is then thermally broadened via collisions [11]. Alternatively, a weaker flux towards the edges of galaxy clusters would match the dark matter density profiles [10].

Unfortunately, Hitomi only operated for a month before malfunctioning. During its time gathering data, it was covered with a protective filter which absorbed most of the x-rays below 5 keV and therefore it did not take enough data around 3.5 keV to identify and resolve the anomalous line, and we will not be able to pinpoint the mechanism for the generation of these x-rays until another mission goes up in the 2020s.

If a future satellite identifies dark matter as the culprit for the line, physics will undergo a revolution. There are several dark matter candidates, besides sterile neutrinos, and all of our attention would shift to identifying and independently measuring the right one. For instance, we could look for keV sterile neutrinos emitted in more sensitive β decays; the electron spectrum would have a kink if some energy is stored in the mass of a sterile neutrino.

Figure 1.1 shows the current parameter space, as dictated by x-ray observations, for the sterile neutrino mass m_s and mixing angle θ (commonly expressed as $\sin^2 2\theta$). The neutrino flavor eigenstates and mass eigenstates are not the same. The flavor and mass eigenbases are “rotated” relative to each other by a mixing angle θ . The bulls-eye for the mass seems to lie around 7.1 keV.

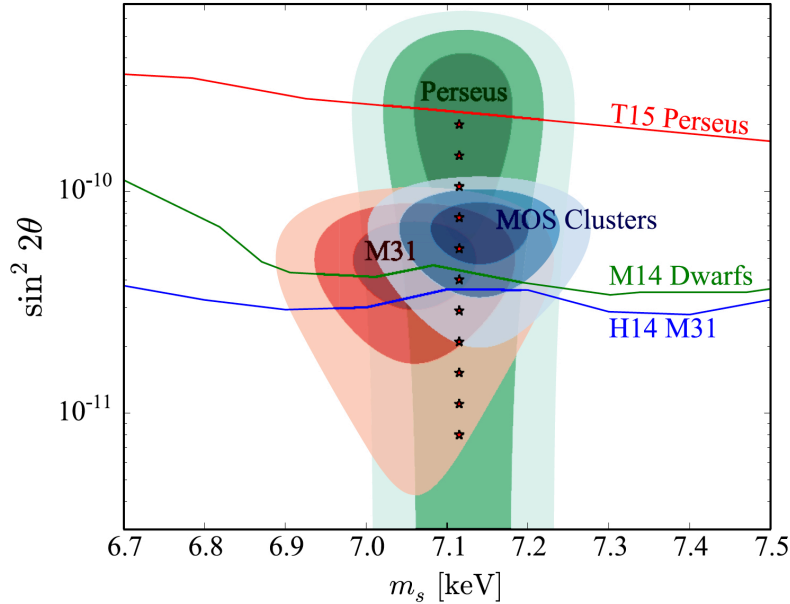


Figure 1.1. Sterile neutrino dark matter parameter space adopted with permission from [32]. The shaded regions are consistent with the x-ray signal at 1, 2, and 3σ . The blue contours come from a stacked spectrum of 73 clusters obtained with the MOS detectors on XMM Netwon. Statistically consistent signals are found in the Perseus spectrum and M31. The lines show constraints at the 90% level from *Chandra* observations of M31, stacked dwarf galaxies, and *Suzaku* observations of Perseus. The stars mark the models studied by [32]

1.3 NEUTRINO COSMOLOGY

In 1929, Edwin Hubble observed that distant galaxies are receding from us and that their recession velocity is proportional to their distance from us: $v = \mathcal{H}d$ [22]. The proportionality factor \mathcal{H} is the Hubble parameter. The physical distance d can be expressed as $d = a(t)r$, where r denotes the comoving coordinate, or the time-independent distance measured in a frame moving together with the expanding Universe, and $a(t)$ is the scale factor. With this substitution, Hubble's discovery becomes

$$\dot{a} = \mathcal{H}a. \quad (1.1)$$

where the dot derivative means d/dt . The evolution of the scale factor, or equivalently the Hubble parameter (today $H_0 = 67.8 \pm 0.9$ km/s Mpc [4]), in a homogeneous and isotropic universe, is governed by general relativity and was derived by Alexander Friedman in 1922 [17]. For a spatially flat universe, it has a particularly simple form,

$$\mathcal{H}^2 = \left(\frac{\dot{a}}{a}\right)^2 = \frac{8\pi G\rho}{3} + \frac{\Lambda}{3} \quad (1.2)$$

$$\mathcal{H}^2 + \dot{\mathcal{H}} = \frac{\ddot{a}}{a} = -\frac{4\pi G}{3}(\rho + 3p) + \frac{\Lambda}{3} \quad (1.3)$$

where G is Newton's constant, ρ is the matter and radiation energy density, and Λ is the cosmological constant, or the vacuum energy density. Throughout this thesis, we set $c = k_B = \hbar = 1$. To be exact, this ought to be interpreted as a background solution, with statistically isotropic and homogeneous perturbations around it. After all, the Universe is irregular and anisotropic on small scales. Simplifying equation 1.2 and differentiating yields,

$$\dot{\mathcal{H}} = \frac{4\pi G\dot{\rho}}{3\mathcal{H}}. \quad (1.4)$$

which, when combined with equation 1.3, results in

$$\dot{\rho} = -3\mathcal{H}(\rho + p). \quad (1.5)$$

Upon substituting a general equation of state $p = w\rho$, where w is a time-independent parameter, and integrating, we arrive at a very important statement about the energy density. Namely,

$$\rho \sim a^{-3(1+w)}. \quad (1.6)$$

In the early Universe, radiation (or relativistic particles) dominated the expansion rate. In such a case, $w = 1/3$, $\rho \sim a^{-4}$, and the evolution of the scale factor is given by

$$\mathcal{H}^2 = \left(\frac{\dot{a}}{a}\right)^2 \sim a^{-4}. \quad (1.7)$$

This is a simple differential equation with the solution

$$a \sim t^{1/2}. \quad (1.8)$$

This implies that the radiation energy density is

$$\rho = \left(\frac{3}{32\pi G} \right) t^{-2}. \quad (1.9)$$

Furthermore, radiation in equilibrium, an easily satisfiable condition in the hot and dense medium in the early Universe, has a simple dependence on temperature. For bosons,

$$\rho = \int g_B f \mathcal{E} \frac{d^3 p}{(2\pi)^3} = \frac{g_B T^4}{2\pi^2} \int_0^\infty \frac{x^3 dx}{e^x - 1} = \left(\frac{g\pi^2}{30} \right) T^4, \quad (1.10)$$

where \mathcal{E} is the relativistic energy, g_B is the bosonic statistical weight and we used the Bose-Einstein distribution $f = (e^{\mathcal{E}/T} - 1)^{-1}$. For fermions, the distribution function is $f = (e^{\mathcal{E}/T} + 1)^{-1}$, and if they are relativistic then

$$\rho = \frac{g_F T^4}{2\pi^2} \int_0^\infty \frac{x^3 dx}{e^x + 1} = \frac{7}{8} \left(\frac{g_F \pi^2}{30} \right) T^4, \quad (1.11)$$

where g_F is the fermionic statistical weight. The total energy density (including both bosons and fermions) is

$$\rho = \left(\frac{g_* \pi^2}{30} \right) T^4, \quad (1.12)$$

where the effective number of degrees of freedom is

$$g_* = \left(\sum_B g_B + \frac{7}{8} \sum_F g_F \right). \quad (1.13)$$

Equating the two forms of ρ gives us a correspondence between time and temperature:

$$T = \left(\frac{45}{16g_* \pi^3 G} \right)^{1/4} t^{-1/2}. \quad (1.14)$$

This result is often quoted as

$$T \approx 1.31 \text{ MeV} \left(\frac{t}{1 \text{ s}} \right)^{-1/2} \approx 1.52 \times 10^{10} \text{ K} \left(\frac{t}{1 \text{ s}} \right)^{-1/2}. \quad (1.15)$$

At temperatures greater than a few GeV, photons, gluons, massive bosons, quarks/antiquarks, leptons/antileptons, neutrinos/antineutrinos pervaded the universe. Accounting for all of their degrees of freedom gives $g_* = 28 + (7/8) \times 90 = 106.75$.

1.4 NEUTRINO DECOUPLING

As the temperature fell, fewer and fewer particle species remained relativistic and around a few MeV only photons, e^\pm , and neutrinos and antineutrinos contributed to the radiation energy density. During this epoch, $g_* = 2 + (7/8) \times 10 = 10.75$. The scattering rate for the process

$$\gamma + \gamma \leftrightarrow e^+ + e^- \leftrightarrow \nu_\alpha + \bar{\nu}_\alpha \quad (1.16)$$

scaled as $\Gamma \sim G_F^2 T^5$ - here $\alpha = e, \mu, \tau$ and G_F is the Fermi constant - and the Universe expanded at a rate of $\mathcal{H} \sim \sqrt{g_*} T^2 / M_{PL}$. Once the scattering rate became less than the expansion rate the neutrinos decoupled from the surrounding plasma and continued to simply redshift with cosmic expansion. This “freeze-out” happened at a temperature of

$$T \sim \left(\frac{\sqrt{g_*}}{G_F^2 M_{PL}} \right)^{1/3} \sim 1 \text{ MeV}. \quad (1.17)$$

After neutrino decoupling, the remaining electrons and positrons annihilate,

$$e^+ + e^- \rightarrow \gamma + \gamma, \quad (1.18)$$

and reheat the still equilibrated photons. The exact amount by which the photons are reheated relative to the neutrinos can be found via entropy conservation. Using the first law of thermodynamics we can get a fundamental relation for entropy density. Namely

$$s = (p + \rho) / T \quad (1.19)$$

where p is the pressure and ρ is the density. Before the annihilation of electrons and positrons, $g_* = 2 + (7/8) \times 4 = 11/2$ and the entropy density is

$$s = \left(\frac{11}{2} \right) \left(\frac{2\pi^2 T^3}{45} \right). \quad (1.20)$$

After the pair annihilation, the entropy density is

$$s = 2 \left(\frac{2\pi^2 T^3}{45} \right). \quad (1.21)$$

Equating the entropies at these two points results in

$$T_\nu = \left(\frac{4}{11} \right)^{1/3} T_\gamma \quad (1.22)$$

Today the Cosmic Microwave Background has a temperature of $T_\gamma = 2.725$ K. This means that the Cosmic Neutrino Background, although still undetected, has a temperature of $T_\nu = 1.945$ K.

Using the ratio of photon and neutrino temperatures we can recast the radiation energy density into

$$\rho = \left(1 + \frac{7}{8} \left(\frac{4}{11} \right)^{4/3} N_{\text{eff}} \right) \rho_{\gamma}, \quad (1.23)$$

where N_{eff} is defined to be the effective number of neutrino species in the early Universe and it equals 3 if there are three massless neutrinos that decoupled instantly. In reality, neutrinos are not massless and they did not decouple instantly, and $N_{\text{eff}} \geq 3$. Much research has gone into analyzing how physics beyond the Standard Model like scattering and oscillations with sterile neutrinos affect N_{eff} .

It should be noted that this discussion of neutrino decoupling neglects neutrino oscillations. Therefore, accounting for neutrino oscillations and perhaps extra neutrino species can change the relic neutrino density and affect Big Bang Nucleosynthesis.

At large temperatures and frequent scattering with the primeval plasma the sterile neutrinos had an equilibrium Fermi-Dirac phase space distribution

$$f = \left(e^{x-\eta} + 1 \right)^{-1} \quad (1.24)$$

where $x = p/T$ and $\eta = \mu/T$ are the scaled momentum and degeneracy parameter. The chemical potential characterizes the neutrino - antineutrino asymmetry. As temperatures fell, this distribution became distorted with higher contributions at lower x , the weak interaction rate fell below the expansion rate and the neutrinos decoupled. This happened at roughly $T \sim 1$ MeV. Since regular neutrinos are nearly massless, they must have contributed to the relativistic energy density at weak decoupling.

After weak decoupling, the electrons and positrons annihilate and reheat the photons. The ratio of the relic photon and neutrino temperatures is $T_{\gamma}/T_{\nu} \approx 1.4$.

Since neutrino decoupling and pair annihilation follow each other closely the above discussion is not entirely true. Neutrinos, in particular the more energetic ones, continued to interact with electrons even after “decoupling.” Therefore, $N_{\text{eff}} > 3$ and the relic neutrino spectrum is distorted (not thermal). We also know (from observations of the CMB) that $N_{\text{eff}} < 4$. Therefore, if sterile neutrinos exist they could not have been in equilibrium with the primordial plasma at weak decoupling.

1.5 BIG BANG NUCLEOSYNTHESIS

Primordial nucleosynthesis and the CMB are the main observational pillars of the hot Big Bang. It is a theory describing how, in just a few minutes, protons and neutrons fused to form the light elements. Because the early universe cooled too quickly, the fusion of heavier elements had to wait until the formation of the first stars.

The synthesis of the light elements started at roughly 1 MeV and lasted until about 10 keV [33]. During this period, the effective number of degrees of freedom g_* dropped from 10.75 (photons, electrons, neutrinos, and their relative antiparticles) to 3.36. Before neutrino decoupling neutrons and protons interconverted in thermal equilibrium and their ratio was

$$\frac{n_n}{n_p} \sim e^{-Q/T}, \quad (1.25)$$

where $Q = m_n - m_p = 1.3$ MeV. Although this approximation is crude and assumes that the chemical potential is zero, the conclusions of this discussion still hold. For a “freeze-out” temperature $T \approx 1$ MeV, the neutron to proton ratio is $n_n/n_p \approx 1/6$. After freeze-out the remaining neutrons decayed into protons until the onset of nucleosynthesis. During nucleosynthesis the ratio falls off precipitously

$$\frac{n_n}{n_p} \sim e^{-Q/T_d} e^{-t/\tau}, \quad (1.26)$$

where $T_d \sim 1$ MeV is the neutrino decoupling temperature, $t \sim (\text{MeV}/T)^2$ s is the time-temperature relation for a radiation dominated universe and $\tau \approx 880$ s is the neutron lifetime. By $T \approx 0.09$ MeV, the ratio falls to $n_n/n_p \approx 0.14$, and nearly all the free neutrons fused into ^4He . The primordial mass fraction of ^4He is

$$Y_p = \frac{m_{He} n_{He}}{m_N (n_p + n_n)}. \quad (1.27)$$

Using $m_{He} \approx 4m_N$, where $m_N \approx m_p \approx m_n \approx 0.94$ GeV is the typical mass of a nucleon, $n_{He} \approx n_n/2$, and $n_n/n_p \approx 0.14$, the mass fraction becomes $Y_p \approx 0.246$.

One can observe the ^4He abundance in the ionized gas of metal-deficient galaxies where the interstellar medium has not been sprinkled with heavier elements produced through stellar burning and its value agrees with Big Bang nucleosynthesis [23].

1.6 VACUUM MIXING

To understand the evolution of active and sterile neutrino ensembles in the early universe, we must first understand a single neutrino oscillating in a vacuum. Then, we will consider oscillations in a medium. And finally, we will make a connection to the evolution of neutrino distributions in the early universe.

To start, consider a 2×2 vacuum mixing of an electron neutrino ν_e and some other active neutrino ν_x

$$\begin{pmatrix} \nu_e \\ \nu_x \end{pmatrix} = \begin{pmatrix} \cos \theta & \sin \theta \\ -\sin \theta & \cos \theta \end{pmatrix} \begin{pmatrix} \nu_1 \\ \nu_2 \end{pmatrix}, \quad (1.28)$$

where ν_1 and ν_2 are the mass eigen states and θ is the mixing angle. This means that the flavor states do not coincide with the mass states. The time evolution of a state initially $|\nu_e\rangle$ is given by

$$|\nu_e(t)\rangle = e^{-i\mathcal{E}_1 t} \cos \theta |\nu_1\rangle + e^{-i\mathcal{E}_2 t} \sin \theta |\nu_2\rangle, \quad (1.29)$$

and the probability of converting to ν_x is

$$P_{\nu_e \rightarrow \nu_x} = |\langle \nu_x | \nu_e(t) \rangle|^2 = \left| \left(-\sin \theta \langle \nu_1 | + \cos \theta \langle \nu_2 | \right) |\nu_e(t)\rangle \right|^2 \quad (1.30)$$

$$= \left| \sin \theta \cos \theta \left(-e^{-i\mathcal{E}_1 t} + e^{-i\mathcal{E}_2 t} \right) \right|^2 \quad (1.31)$$

$$= \left| \sin \theta \cos \theta \left(e^{-i(\mathcal{E}_1 + \mathcal{E}_2) \frac{t}{2}} \left(e^{\frac{\Delta \mathcal{E} t}{2}} - e^{-\frac{\Delta \mathcal{E} t}{2}} \right) \right) \right|^2 \quad (1.32)$$

$$= \left| 2i \sin \theta \cos \theta \sin (\Delta \mathcal{E} t / 2) \right|^2 = \left(\sin 2\theta \times \sin (\Delta \mathcal{E} t / 2) \right)^2. \quad (1.33)$$

For relativistic energies this simplifies to

$$P_{\nu_e \rightarrow \nu_x} = \left(\sin 2\theta \times \sin \left(\frac{\delta m^2 L}{4\mathcal{E}} \right) \right)^2 = \left(\sin 2\theta \times \sin \left(\frac{1.27 \delta m^2 L}{4\mathcal{E}_\nu} \right) \right)^2. \quad (1.34)$$

where L is the neutrino propagation distance and we rescaled the units to meters and MeV. In other words, the survival probability of an electron neutrino is

$$P_{\nu_e} = 1 - \left(\sin 2\theta \times \sin \left(\frac{1.27 \delta m^2 L}{4\mathcal{E}_\nu} \right) \right)^2. \quad (1.35)$$

Figure 1.2 shows the application of this model to muon neutrinos in the atmosphere for which the mixing angle is $\sin^2 2\theta = 0.92$ and the mass splitting is $\delta m^2 = 2.4 * 10^{-3} \text{ eV}$ [18].

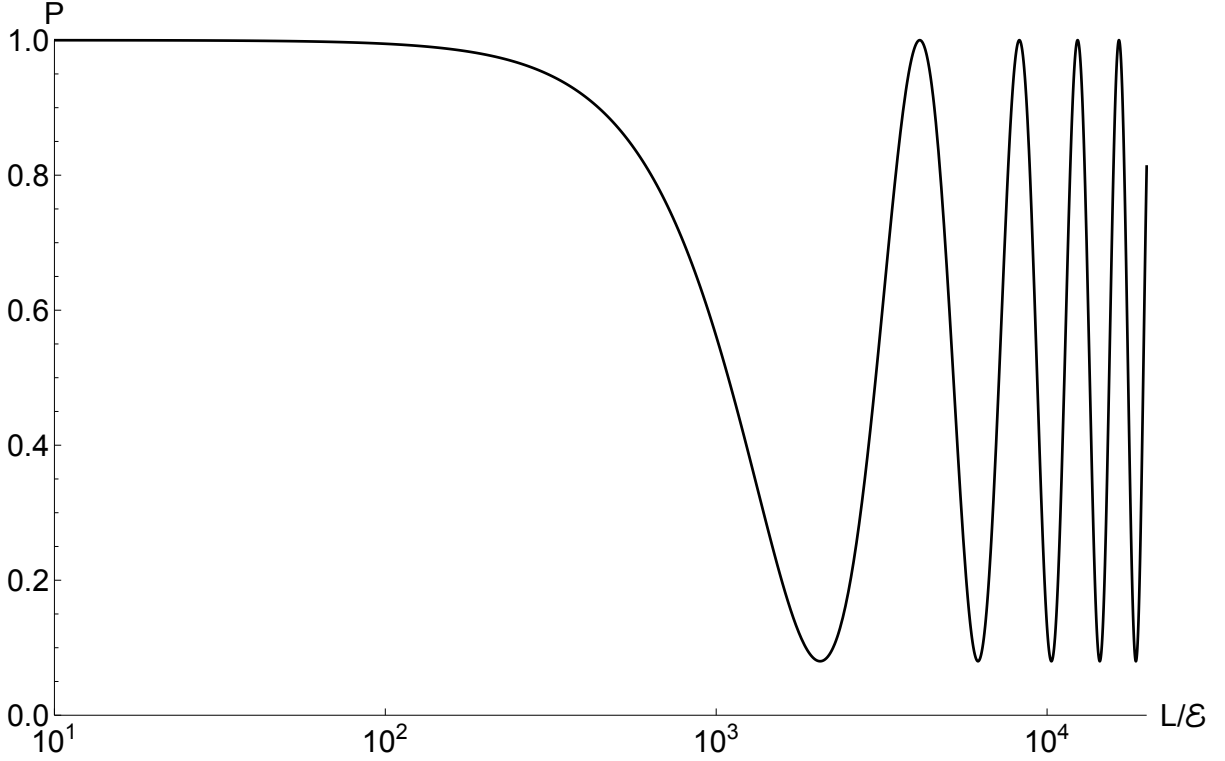


Figure 1.2. Survival probability P_{ν_μ} vs. [meters/MeV] for $\nu_\mu \leftrightarrow \nu_\tau$ oscillations for $\delta m^2 = 2.4 * 10^{-3}$ eV and $\sin^2 2\theta = 0.92$.

1.7 IN MEDIUM MIXING

It is simple to generalize this to include the effects of a surrounding medium. The important takeaway will be that, in a medium, neutrino oscillations can resonate [28]. For convenience, we will continue the discussion in the mass basis, which is simply recovered by inverting the flavor basis.

$$\begin{pmatrix} \nu_e \\ \nu_x \end{pmatrix} = \begin{pmatrix} \cos \theta & \sin \theta \\ -\sin \theta & \cos \theta \end{pmatrix} \begin{pmatrix} \nu_1 \\ \nu_2 \end{pmatrix} \Longleftrightarrow \begin{pmatrix} \nu_1 \\ \nu_2 \end{pmatrix} = \begin{pmatrix} \cos \theta & -\sin \theta \\ \sin \theta & \cos \theta \end{pmatrix} \begin{pmatrix} \nu_e \\ \nu_x \end{pmatrix} \quad (1.36)$$

In the flavor basis, the kinetic energy operator is

$$T = \mathcal{E}_1 |\nu_1\rangle \langle \nu_1| + \mathcal{E}_2 |\nu_2\rangle \langle \nu_2| \quad (1.37)$$

$$= \begin{pmatrix} \mathcal{E}_1 \cos^2 \theta + \mathcal{E}_2 \sin^2 \theta & -\sin \theta \cos \theta (\mathcal{E}_1 + \mathcal{E}_2) \\ -\sin \theta \cos \theta (\mathcal{E}_1 + \mathcal{E}_2) & \mathcal{E}_2 \cos^2 \theta - \mathcal{E}_1 \sin^2 \theta \end{pmatrix} \quad (1.38)$$

$$= \frac{\mathcal{E}_1 + \mathcal{E}_2}{2} \begin{pmatrix} 1 & 0 \\ 0 & 1 \end{pmatrix} + \frac{\Delta \mathcal{E}}{2} \begin{pmatrix} -\cos 2\theta & \sin 2\theta \\ \sin 2\theta & \cos 2\theta \end{pmatrix}. \quad (1.39)$$

Electron neutrinos have both charged current and neutral current forward scattering with electrons, unlike the other neutrinos which have only neutral current interactions with electrons. This means that the Hamiltonian has an extra potential term U_e which is proportional to the electron density in the medium. In other words,

$$U = \begin{pmatrix} U_e & 0 \\ 0 & 0 \end{pmatrix} = \frac{U_e}{2} \begin{pmatrix} 1 & 0 \\ 0 & 1 \end{pmatrix} + \frac{U_e}{2} \begin{pmatrix} 1 & 0 \\ 0 & -1 \end{pmatrix}, \quad (1.40)$$

and the Hamiltonian is

$$\mathcal{H} = \left(\frac{\mathcal{E}_1 + \mathcal{E}_2 + U_e}{2} \right) \begin{pmatrix} 1 & 0 \\ 0 & 1 \end{pmatrix} + \frac{\Delta\mathcal{E}}{2} \begin{pmatrix} -\cos 2\theta & \sin 2\theta \\ \sin 2\theta & \cos 2\theta \end{pmatrix} + \frac{U_e}{2} \begin{pmatrix} 1 & 0 \\ 0 & -1 \end{pmatrix}. \quad (1.41)$$

The first term proportional to the identity matrix is irrelevant to neutrino flavor conversion and we will neglect it in deriving the effective mass and mixing angle. The two terms can be combined giving

$$\mathcal{H} = \dots + \frac{\delta\tilde{m}^2}{4\mathcal{E}} \begin{pmatrix} -\cos 2\theta_M & \sin 2\theta_M \\ \sin 2\theta_M & \cos 2\theta_M \end{pmatrix}. \quad (1.42)$$

Here \tilde{m} and θ_M are the "effective" in medium mass and angle. They are defined in terms of the vacuum mass and angle as

$$\frac{\delta\tilde{m}^2}{4\mathcal{E}} \cos 2\theta_M = \frac{\delta m^2}{4\mathcal{E}} \cos 2\theta - \frac{U_e}{2} \quad (1.43)$$

$$\frac{\delta\tilde{m}^2}{4\mathcal{E}} \sin 2\theta_M = \frac{\delta m^2}{4\mathcal{E}} \sin 2\theta. \quad (1.44)$$

Combining these two equations allows us to define θ_M

$$\tan 2\theta_M = \frac{\tan 2\theta}{\left(1 - \frac{2\mathcal{E}U_e}{\delta m^2 \cos 2\theta}\right)}, \quad (1.45)$$

and \tilde{m}

$$\delta\tilde{m}^2 \left(\cos^2 2\theta_M + \sin^2 2\theta_M \right)^{\frac{1}{2}} = \left[\left(\delta m^2 \cos 2\theta - 2\mathcal{E}U_e \right)^2 + \left(\delta m^2 \sin 2\theta \right)^2 \right]^{\frac{1}{2}} \quad (1.46)$$

$$\delta\tilde{m}^2 = \left[\left(\delta m^2 \cos 2\theta - 2\mathcal{E}U_e \right)^2 + \left(\delta m^2 \sin 2\theta \right)^2 \right]^{\frac{1}{2}}. \quad (1.47)$$

In analogy to vacuum oscillations, the "in medium" mixing probability, in terms of the effective mass and angle, is

$$P_{\nu_e \rightarrow \nu_x} = \left[\sin 2\theta_M \times \sin \left(\frac{\delta\tilde{m}^2 L}{4\mathcal{E}_\nu} \right) \right]^2 \quad (1.48)$$

The important distinction is that this probability, unlike the vacuum, has resonances given by

$$\delta m^2 \cos 2\theta = 2\mathcal{E}U_e. \quad (1.49)$$

1.8 ADIABATIC IN MEDIUM MIXING

Another important feature of adiabatic in medium oscillations of a single neutrino is that its mass state remains pure. To see this, let us use the Hamiltonian derived in the previous section to write out the equations of motion. In the flavor basis, they are

$$i \begin{pmatrix} \dot{\nu}_e \\ \dot{\nu}_x \end{pmatrix} = \mathcal{H} \begin{pmatrix} \nu_e \\ \nu_x \end{pmatrix} = \left\{ \frac{\delta \tilde{m}^2}{4\mathcal{E}} \begin{pmatrix} -\cos 2\theta_M & \sin 2\theta_M \\ \sin 2\theta_M & \cos 2\theta_M \end{pmatrix} \right\} \begin{pmatrix} \nu_e \\ \nu_x \end{pmatrix} \quad (1.50)$$

We will refer to $\cos 2\theta_M$ and $\sin 2\theta_M$ as c and s , respectively, for notational convenience. In the mass basis, the evolution is given by

$$i \frac{d}{dt} \left[\begin{pmatrix} c & s \\ -s & c \end{pmatrix} \begin{pmatrix} \nu_1 \\ \nu_2 \end{pmatrix} \right] = \left\{ \dots \right\} \begin{pmatrix} c & s \\ -s & c \end{pmatrix} \begin{pmatrix} \nu_1 \\ \nu_2 \end{pmatrix} \quad (1.51)$$

where $\{\dots\}$ is shorthand for the first term on the RHS. The derivative on the LHS expands to

$$i \left[\dot{\theta}_M \begin{pmatrix} -s & c \\ -c & -s \end{pmatrix} \begin{pmatrix} \nu_1 \\ \nu_2 \end{pmatrix} + \begin{pmatrix} c & s \\ -s & c \end{pmatrix} \begin{pmatrix} \dot{\nu}_1 \\ \dot{\nu}_2 \end{pmatrix} \right] = \dots \quad (1.52)$$

Moving $\dot{\theta}_M$ to the RHS and multiplying everything by $\begin{pmatrix} c & -s \\ s & c \end{pmatrix}$ gives

$$\begin{pmatrix} c & -s \\ s & c \end{pmatrix} \left[i \begin{pmatrix} c & s \\ -s & c \end{pmatrix} \begin{pmatrix} \dot{\nu}_1 \\ \dot{\nu}_2 \end{pmatrix} = \left\{ \dots \right\} \begin{pmatrix} c & s \\ -s & c \end{pmatrix} \begin{pmatrix} \nu_1 \\ \nu_2 \end{pmatrix} - i \dot{\theta}_M \begin{pmatrix} -s & c \\ -c & -s \end{pmatrix} \begin{pmatrix} \nu_1 \\ \nu_2 \end{pmatrix} \right]. \quad (1.53)$$

Finally, this expression simplifies to

$$i \begin{pmatrix} \dot{\nu}_1 \\ \dot{\nu}_2 \end{pmatrix} = \frac{\delta \tilde{m}^2}{4\mathcal{E}} \begin{pmatrix} -1 & 0 \\ 0 & 1 \end{pmatrix} \begin{pmatrix} \nu_1 \\ \nu_2 \end{pmatrix} - i \dot{\theta}_M \begin{pmatrix} 0 & 1 \\ -1 & 0 \end{pmatrix} \begin{pmatrix} \nu_1 \\ \nu_2 \end{pmatrix}. \quad (1.54)$$

These algebraic gymnastics grant us an important insight. In the mass basis, it becomes evident that an adiabatic evolution ($\dot{\theta}_M \ll \delta \tilde{m}^2 / 4\mathcal{E}$) prevents switching of mass states. In other words, if a neutrino starts in a stationary state ν_1 , it will remain in ν_1 even as it traverses a medium of variable density. In other words, if $4\mathcal{E}\dot{\theta}_M / \tilde{m}^2 \ll 1$ then

$$i \begin{pmatrix} \dot{\nu}_1 \\ \dot{\nu}_2 \end{pmatrix} = \frac{\delta \tilde{m}^2}{4\mathcal{E}} \begin{pmatrix} -1 & 0 \\ 0 & 1 \end{pmatrix} \begin{pmatrix} \nu_1 \\ \nu_2 \end{pmatrix} \quad (1.55)$$

and the differential equations for ν_1 and ν_2 are independent.

1.9 QUANTUM KINETIC EQUATIONS

The evolution of an ensemble of active and sterile neutrinos is often modeled using the density operator for a neutrino of a certain scaled momentum $x = p/T$ [27].

$$\rho = \sum_{i,j} \rho_{ij} |\nu_i\rangle \langle \nu_j| = \rho_{ee} |\nu_e\rangle \langle \nu_e| + \rho_{es} |\nu_e\rangle \langle \nu_s| + \rho_{se} |\nu_s\rangle \langle \nu_e| + \rho_{ss} |\nu_s\rangle \langle \nu_s| \quad (1.56)$$

For simplicity, we consider 2×2 mixing between an active and a sterile neutrino [24]. The weak eigenstates are $|\nu_e\rangle$ and $|\nu_s\rangle$, and the energy-mass eigenstates are $|\nu_1\rangle$ and $|\nu_2\rangle$.

$$\begin{pmatrix} \nu_e \\ \nu_s \end{pmatrix} = \begin{pmatrix} \cos \theta & \sin \theta \\ -\sin \theta & \cos \theta \end{pmatrix} \begin{pmatrix} \nu_1 \\ \nu_2 \end{pmatrix} \quad (1.57)$$

In this case,

$$\rho = \begin{pmatrix} \rho_{ee}(1 - \sin 2\theta) & \rho_{es} \cos 2\theta \\ \rho_{se} \cos 2\theta & \rho_{ss}(1 + \sin 2\theta) \end{pmatrix} \quad (1.58)$$

It is convenient to recast the density operator in terms of polarization vectors and Pauli matrices

$$\rho = \frac{1}{2} P_0 (\mathbb{1} + \mathbf{P} \cdot \boldsymbol{\sigma}) \quad (1.59)$$

where

$$\sigma_x = \begin{pmatrix} 0 & 1 \\ 1 & 0 \end{pmatrix} \quad \sigma_y = \begin{pmatrix} 0 & -i \\ i & 0 \end{pmatrix} \quad \sigma_z = \begin{pmatrix} 1 & 0 \\ 0 & -1 \end{pmatrix} \quad (1.60)$$

In other words,

$$\rho = \frac{1}{2} P_0 \begin{pmatrix} 1 + P_z & P_x - iP_y \\ P_x + iP_y & 1 - P_z \end{pmatrix} \quad (1.61)$$

To justify rewriting the density operator in a Pauli basis, consider the following, generic matrix.

$$\rho = \begin{pmatrix} a & b \\ c & d \end{pmatrix} = a \begin{pmatrix} 1 & 0 \\ 0 & 0 \end{pmatrix} + d \begin{pmatrix} 0 & 0 \\ 0 & 1 \end{pmatrix} + b \begin{pmatrix} 0 & 1 \\ 0 & 0 \end{pmatrix} + c \begin{pmatrix} 0 & 0 \\ 1 & 0 \end{pmatrix} \quad (1.62)$$

The basis for this matrix is

$$\left\{ \begin{pmatrix} 1 & 0 \\ 0 & 0 \end{pmatrix}, \begin{pmatrix} 0 & 0 \\ 0 & 1 \end{pmatrix}, \begin{pmatrix} 0 & 1 \\ 0 & 0 \end{pmatrix}, \begin{pmatrix} 0 & 0 \\ 1 & 0 \end{pmatrix} \right\} \quad (1.63)$$

Adding and subtracting the first two entries, and the third and fourth entries recasts the basis into

$$\left\{ \begin{pmatrix} 1 & 0 \\ 0 & 1 \end{pmatrix}, \begin{pmatrix} 1 & 0 \\ 0 & -1 \end{pmatrix}, \begin{pmatrix} 0 & 1 \\ 1 & 0 \end{pmatrix}, \begin{pmatrix} 0 & 1 \\ -1 & 0 \end{pmatrix} \right\} \quad (1.64)$$

The first three entries are Hermitian, whereas the fourth must be rescaled by $-i$ to ensure that the density matrix is Hermitian. In other words, ρ can be written using the following basis

$$\left\{ \begin{pmatrix} 1 & 0 \\ 0 & 1 \end{pmatrix}, \begin{pmatrix} 1 & 0 \\ 0 & -1 \end{pmatrix}, \begin{pmatrix} 0 & 1 \\ 1 & 0 \end{pmatrix}, \begin{pmatrix} 0 & -i \\ i & 0 \end{pmatrix} \right\} = \{\mathbb{1}, \sigma_z, \sigma_x, \sigma_y\} \quad (1.65)$$

Now, it is clear why we can say that the density operator is

$$\rho = \frac{1}{2}P_0(\mathbb{1} + \mathbf{P} \cdot \boldsymbol{\sigma}) \quad (1.66)$$

In this picture, \mathbf{P} acts as a polarization vector and P_0 is a normalization factor proportional to the total number density of all neutrinos. The diagonal matrix elements of ρ are proportional to the individual number densities of active and sterile neutrinos. In other words, $\text{Tr}(\rho) = P_0$ and

$$\rho_{\alpha\alpha} = \frac{1}{2}P_0(1 + P_z) \equiv f_\alpha \quad (1.67)$$

$$\rho_{ss} = \frac{1}{2}P_0(1 - P_z) \equiv f_s \quad (1.68)$$

When multiplied by the zero chemical potential Fermi-Dirac distribution the diagonal entries give the number densities of active and sterile neutrinos.

$$n_\alpha = f_\alpha \left(\frac{T^3}{2\pi^2} \frac{x^2}{e^x + 1} \right) \quad (1.69)$$

$$n_s = f_s \left(\frac{T^3}{2\pi^2} \frac{x^2}{e^x + 1} \right) \quad (1.70)$$

For a homogeneous and isotropic universe, we can derive the equations governing the evolution of both the active and sterile neutrino densities. Below, we simply state these quantum kinetic equations, and in the next section we give a heuristic motivation for their form [27].

$$\dot{\mathbf{P}} = \mathbf{V} \times \mathbf{P} + (1 - P_z)(\dot{P}_0/P_0)\hat{z} - (\mathcal{D} + (\dot{P}_0/P_0))\mathbf{P}_\perp \quad (1.71)$$

$$\dot{P}_0 = \Gamma \left(\frac{e^x + 1}{e^{x-\eta} + 1} - f_\alpha \right) \quad (1.72)$$

The \dot{P}_0 equation describes scattering in and out of active and sterile neutrino states and it drives the distribution of active neutrinos to a Fermi-Dirac spectrum consistent with a lepton asymmetry,

$$n \propto f\left(\frac{x^2}{e^x + 1}\right) \rightarrow \frac{x^2}{e^{x-\eta} + 1} \quad (1.73)$$

The form of \dot{P}_0 stated above assumes that all other species, besides ν_e and ν_s , are in equilibrium, and is valid at temperatures above neutrino decoupling. This ensures that active neutrinos can exchange energy and momentum with the plasma. The transverse polarization vector is $\mathbf{P}_\perp = P_x \hat{x} + P_y \hat{y}$. The scaled chemical potential, sometimes referred to as the degeneracy parameter, is $\eta = \mu/T$. The Hamiltonian responsible [2] for the coherent evolution of the neutrino states is

$$\mathcal{H} = \left(xT + \frac{m_1^2 + m_2^2}{4xT} + \frac{V_e}{2}\right) \mathbb{1} + \frac{1}{2} \mathbf{V} \cdot \boldsymbol{\sigma} \quad (1.74)$$

where

$$\mathbf{V} = \frac{\delta m^2}{2xT} (\sin 2\theta \hat{x} - \cos 2\theta \hat{z}) + V_e \hat{z}. \quad (1.75)$$

The first term describes vacuum mixing, whereas the second term represents the forward scattering potential

$$V_e = \frac{2\sqrt{2}\zeta(3)}{\pi^2} G_F \mathcal{L}_e T^3 - r_e G_F^2 x T^5. \quad (1.76)$$

Since we will consider lepton numbers orders of magnitude larger than the baryon to photon ratio, we neglect neutrino-baryon and neutrino-charged-lepton interactions in the forward scattering potential. The difference of the squares of the vacuum neutrino masses is $\delta m^2 = m_2^2 - m_1^2$, G_F is the Fermi constant, $\zeta(3) \approx 1.20206$, and $r_e = 79.34$ encodes the degrees of freedom of charged leptons [1]. The lepton asymmetry term in the Hamiltonian is

$$\mathcal{L}_e \equiv 2L_e + \sum_{\beta \neq e} L_\beta \quad (1.77)$$

where the individual lepton numbers are defined to be

$$L = \frac{n_{\nu_e} - n_{\bar{\nu}_e}}{n_\gamma} \quad (1.78)$$

where n , \bar{n} , and $n_\gamma = 2\zeta(3)T^3/\pi^2$ are the neutrino, antineutrino, and photon number densities. Assuming thermal equilibrium and neglecting higher order terms on the order of the lepton number, the scattering rate is

$$\Gamma_\alpha \approx y_e G_F^2 x T^5 \quad (1.79)$$

and the decoherence function, responsible for the loss of coherence due to collisions, is half the scattering rate [31].

$$D = \Gamma_\alpha/2 \quad (1.80)$$

The coefficient y_e depends on the number of relativistic particles with a weak charge. At temperatures where most of the scattering is between neutrinos and electron, positron pairs, $y_e \approx 1.27$. At higher temperatures, and higher quark and charged lepton densities, the scattering rate may be higher.

To understand how the lepton asymmetry depends on the chemical potential, remember that the number density of neutrinos is

$$n = \int \frac{d^3p}{(2\pi)^3} f \quad (1.81)$$

This means that the lepton number in its integral form is

$$L = \frac{1}{4\zeta(3)} \int_0^\infty dx x^2 (f - \bar{f}) \quad (1.82)$$

$$= \frac{1}{4\zeta(3)} \int_0^\infty dx x^2 \left(\frac{1}{e^{x-\eta} + 1} - \frac{1}{e^{x+\eta} + 1} \right) \quad (1.83)$$

Evaluating the Fermi Integrals, which have the following form,

$$\mathcal{F}_k(n) = \int_0^\infty dx \frac{x^k}{e^{x-\eta} + 1} \quad (1.84)$$

allows us to write a simple expression for L in terms of the chemical potential

$$L = \frac{\pi^2}{12\zeta(3)} \left(\eta + \frac{\eta^3}{\pi^2} \right) \quad (1.85)$$

We assume that L is initially positive and stored in all the neutrino species. We do not attempt to explain its origin. Experimentally, the limits on the lepton asymmetry are large. Values as large as $L \sim 5 \times 10^{-2}$ are allowed [16]; a full eight orders of magnitude larger than the baryon/photon ratio $n \sim 6 \times 10^{-10}$. This means that further BBN constraints on the lepton number will be crucial for testing models of the early universe. Furthermore, a recently detected x-ray line at 3.5 keV has sparked debate that it may arise from decaying dark matter. If this dark matter is a resonantly produced sterile neutrino in a universe containing a lepton asymmetry, then the flux of the line suggests $L \sim 5 \times 10^{-4}$ [3].

The active and sterile neutrino distributions depend on the lepton asymmetry. Therefore, we need to understand how the lepton asymmetry evolves if we want to evolve the

neutrino densities. We assume the only exotic physics is the active-sterile neutrino oscillations and we posit that the active neutrinos are in thermal equilibrium (at least for $T > 3MeV$). This implies that before neutrino decoupling, the lepton number is

$$\dot{L} = \dot{n}/n_\gamma = -\frac{1}{4\zeta(3)} \int_0^\infty dx \left(\frac{x^2}{e^x + 1} \right) \dot{f} \quad (1.86)$$

where we used

$$\dot{n} = \frac{\partial}{\partial t} \int \frac{d^3p}{(2\pi)^3} f \quad (1.87)$$

Recall, the Friedmann equation for a radiation dominated universe is

$$\mathcal{H}^2 = \left(\frac{\dot{a}}{a} \right)^2 = \frac{8\pi\rho}{3m_{PL}^2} \quad (1.88)$$

where ρ is the total energy density. This means that

$$\left(\frac{\dot{a}}{a} \right)^2 = \frac{4\pi^3 g T^4}{45m_{PL}^2}. \quad (1.89)$$

Since $T = a^{-1}$ and $\dot{T} = -a^{-2} \dot{a}$, the temperature evolution is

$$\dot{T} = - \left(\frac{4\pi^3 g}{45m_{PL}^2} \right)^{\frac{1}{2}} T^3. \quad (1.90)$$

1.10 MOTIVATION OF THE QUANTUM KINETIC EQUATIONS

To understand the behavior of the quantum kinetic equations consider the simplest density matrix

$$\rho = |\psi\rangle \langle\psi| \quad (1.91)$$

Generally, the evolution of a quantum state, or a density matrix, is given by

$$i \left| \dot{\psi} \right\rangle = \mathcal{H} |\psi\rangle \quad (1.92)$$

$$i\dot{\rho} = i \left(\left| \dot{\psi} \right\rangle \langle\psi| + |\psi\rangle \left\langle \dot{\psi} \right| \right) = \mathcal{H}\rho - \rho\mathcal{H}^\dagger \quad (1.93)$$

Recast, using a commutator, the equation becomes

$$i\dot{\rho} = [\mathcal{H}, \rho] + \mathcal{C} \quad (1.94)$$

where \mathcal{H} is the coherent evolution Hamiltonian and \mathcal{C} represents extra physics arising from collisions. Excluding the term proportional to the identity matrix, the Hamiltonian is

$$\mathcal{H} \sim \mathbf{V} \cdot \boldsymbol{\sigma} \quad (1.95)$$

Remembering that

$$\rho = \frac{1}{2}(\mathbb{1} + \mathbf{P} \cdot \boldsymbol{\sigma}) \quad (1.96)$$

and neglecting decoherent scattering, we see that the evolution is given by

$$i\dot{\rho} = [\mathcal{H}, \rho] \quad (1.97)$$

$$= \frac{1}{2} \sum_{jk} (\sigma_j \sigma_k V_j P_k - \sigma_k \sigma_j V_j P_k) \quad (1.98)$$

$$= \frac{1}{2} \sum_{jk} [\sigma_j, \sigma_k] V_j P_k = i (\mathbf{V} \times \mathbf{P}) \cdot \boldsymbol{\sigma} \quad (1.99)$$

In other words,

$$\dot{\mathbf{P}} = \mathbf{V} \times \mathbf{P} \quad (1.100)$$

We used $[\sigma_j, \sigma_k] = 2i \varepsilon_{jkl} \sigma_l$ to simplify equation 1.100. The solution to this differential equation is a precession of \mathbf{P} around \mathbf{V} (Figure 1.3). In other words, in the absence of decoherent scattering the polarization vector \mathbf{P} encircles the Hamiltonian vector \mathbf{V} . Additionally, if \mathbf{V} migrates then \mathbf{P} follows along. If we include coherence disrupting collisions, \mathbf{P} sticks closer to \mathbf{V} and in certain cases does not precess at all. Also, if \mathbf{V} changes nonadiabatically then the leash on \mathbf{P} can be broken. We discuss the geometry of the quantum kinetic equations, particularly at the resonances, in more detail in Chapter 2.

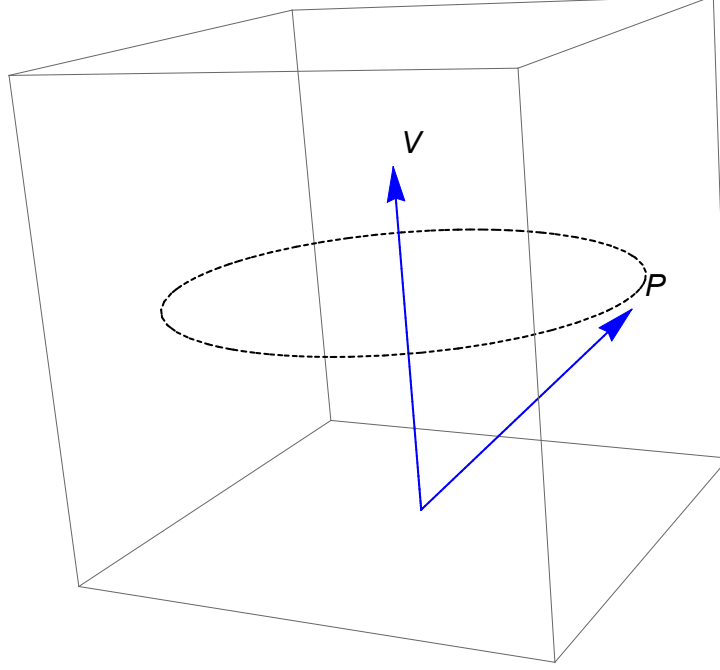


Figure 1.3. Schematic of P precessing around V for the case of a coherent evolution.

1.11 ZENO EQUATIONS

The Zeno approximation posits the following picture. Between collisions, the neutrinos are oscillating in a superposition of states. The collisions collapse these superpositions into either active or sterile states. Crudely put, the collisions act like measurements. This picture is accurate up to a factor of *half*. In other words, the rate of measurement should be *half* the collision frequency [31]. With this in mind, the reaction rate is *half* the interaction rate due to collisions with other particles multiplied by the probability (averaged over an ensemble of neutrinos) of collapsing to a sterile state

$$\Gamma(\nu_e \rightarrow \nu_s) = \frac{\Gamma_{\nu_e}}{2} \langle P_{\nu_e \rightarrow \nu_s} \rangle. \quad (1.101)$$

where

$$\langle P_{\nu_e \rightarrow \nu_s} \rangle = \int_0^\infty \left(\sin 2\theta_M \sin(t/\ell) \right)^2 e^{-\mathcal{D}t} dt \Big/ \int_0^\infty e^{-\mathcal{D}t} dt. \quad (1.102)$$

While streaming through the primordial plasma, neutrinos forward scatter on particles which carry a weak charge and acquire an effective mass much like light gains an effective mass as it traverses glass. In this case, neutrinos also get an effective mixing angle θ_M given by

$$\sin^2 2\theta_M = \frac{\sin^2 2\theta}{\left(\sin^2 2\theta + \left(\cos 2\theta - 2xT V_e / \delta m^2 \right)^2 \right)}, \quad (1.103)$$

where θ is the vacuum mixing angle. In principle, the mixing of three active neutrinos and one sterile neutrino is a complicated unitary transform, but our simple 2×2 approach characterized by a single parameter θ still captures the essence of *how* sterile neutrinos are produced in the early Universe.

Note, the forward scattering potential is

$$V_e = \frac{2\sqrt{2}\zeta(3)}{\pi^2} G_F \mathcal{L}_e T^3 - r_e G_F^2 x T^5 \quad (1.104)$$

where the first term stems from lepton asymmetry and the second is the thermal term. The high temperature sensitivity mean that this term heavily suppresses the effective mixing angle at high T. In this work we consider a large lepton asymmetry and therefore do not generalize the equations to include antineutrinos. The neutrino oscillation length is

$$\ell = \left[\left(\frac{\delta m^2}{2xT} \sin 2\theta \right)^2 + \left(\frac{\delta m^2}{2xT} \cos 2\theta - V_e \right)^2 \right]^{-\frac{1}{2}}, \quad (1.105)$$

and the decoherence function is $\mathcal{D} = \Gamma_{\nu_e}/2$.

Then, the production rate for $\nu_e \leftrightarrow \nu_s$, using the Zeno approximation, is the following statement

$$\frac{\partial f_s}{\partial t} + \left(\frac{dx}{dt} \right) \frac{\partial f_s}{\partial x} = \mathcal{D} \langle P_{\nu_e \rightarrow \nu_s} \rangle (f_e - f_s). \quad (1.106)$$

Although, for a radiation dominated universe,

$$\dot{x} = \left(\frac{x}{3g} \right) \dot{g}, \quad (1.107)$$

we assume g (the sum of the bosonic and fermionic degrees of freedom) is constant even though as species fall out of equilibrium and pair annihilation reheats the universe, g changes.

Evaluating the probability integral, with $\sin^2 2\theta_M$ pulled out, the \dot{f}_s equation takes on the following form [2].

$$\dot{f}_s = \frac{(\mathcal{D}/2) \sin^2 2\theta_M (f_e - f_s)}{(1 + (\mathcal{D} \ell)^2)} \quad (1.108)$$

Nested in \dot{f}_s are evolving lepton numbers and temperatures. The relevant equations are presented in Section 1.9. This differential equation for f_s grants us a snapshot of the relic sterile neutrino energy spectrum

$$f_\nu(x) = f_s(x, T) \left(\frac{x^2}{e^x + 1} \right). \quad (1.109)$$

at any temperature T . Figure 1.4 shows a snapshot of the relic sterile neutrino energy spectrum at $T = 50$ MeV for $m_s = 64$ keV, $\sin^2 \theta = 10^{-10}$, and $L_0 = 1.1 \times 10^{-3}$ that is consistent with [24]. Figure 1.5 shows a spectrum consistent with current x-ray observations [32].

If the scattering time scale is much shorter than the oscillation time scale ($\mathcal{D}^{-1} \ll \ell$), quantum phase cannot accumulate, and transitions between states are suppressed. This suppression of the sterile neutrino production is the quantum Zeno effect. In equation 1.108, this is captured by the denominator

$$\left(1 + (\mathcal{D} \ell)^2\right). \quad (1.110)$$

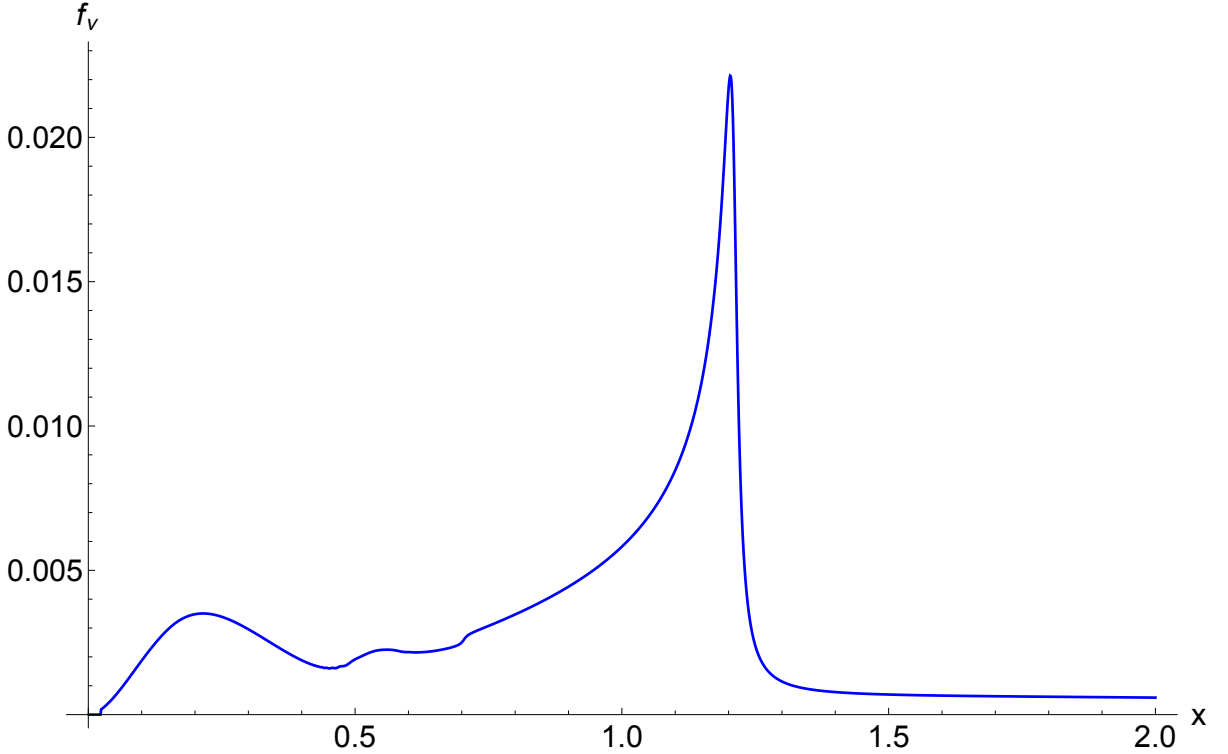


Figure 1.4. A sterile neutrino spectrum at $T = 50$ MeV as a function of scaled momentum x . This evolution is for $m_s = 64$ keV, $\sin^2 \theta = 10^{-10}$, and $L_0 = 1.1 * 10^{-3}$.

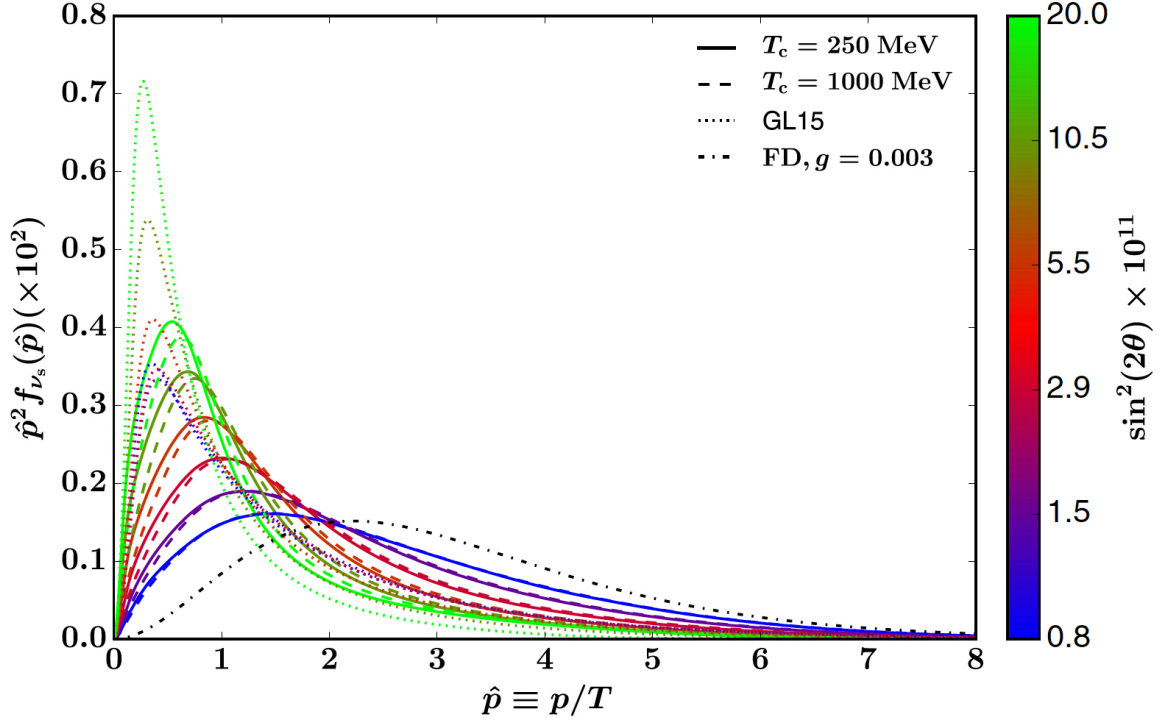


Figure 1.5. A phase space distribution at $T = 10$ MeV for a sterile neutrino mass of $m_s = 7.1$ keV. The mixing angle $\sin^2 2\theta$ is varied and shown in different colors. This figure is adopted with permission from [32] and assumes 2×2 mixing between ν_s and ν_μ . The y-axis is multiplied by a massless Fermi-Dirac distribution with degeneracy $g = 0.003$.

The production of sterile neutrinos is maximal when $\sin^2 2\theta_M = 1$. This corresponds to a quadratic equation for resonant scaled momenta

$$\delta m^2 \cos 2\theta = \frac{4\sqrt{2}\zeta(3)}{\pi^2} G_F \mathcal{L} x T^4 - 2r_e G_F^2 x^2 T^6. \quad (1.111)$$

The solutions are

$$x = \frac{\sqrt{2}\zeta(3)}{\pi^2 r_e G_F T^2} \mathcal{L} \left(1 \pm \sqrt{1 - \frac{\pi^4 r_e \delta m^2 \cos 2\theta}{4\zeta^2(3) \mathcal{L}^2 T^2}} \right). \quad (1.112)$$

For keV sterile neutrinos two resonances occur in the temperature range $\sim 0.1 - 1$ GeV, but this condition is not always met. As the universe expands, both the lepton asymmetry and the temperature decrease (Figure 1.6) and the radical can become imaginary. The lepton number decreases because as electron neutrinos convert to sterile neutrinos they leave holes in the electron neutrino sea which, in an environment striving for equilibrium, are filled by ν_e and $\bar{\nu}_e$ pair production. As the number of electron antineutrinos increases the lepton number $L = (n_{\nu_e} - n_{\bar{\nu}_e})/n_\gamma$ falls.

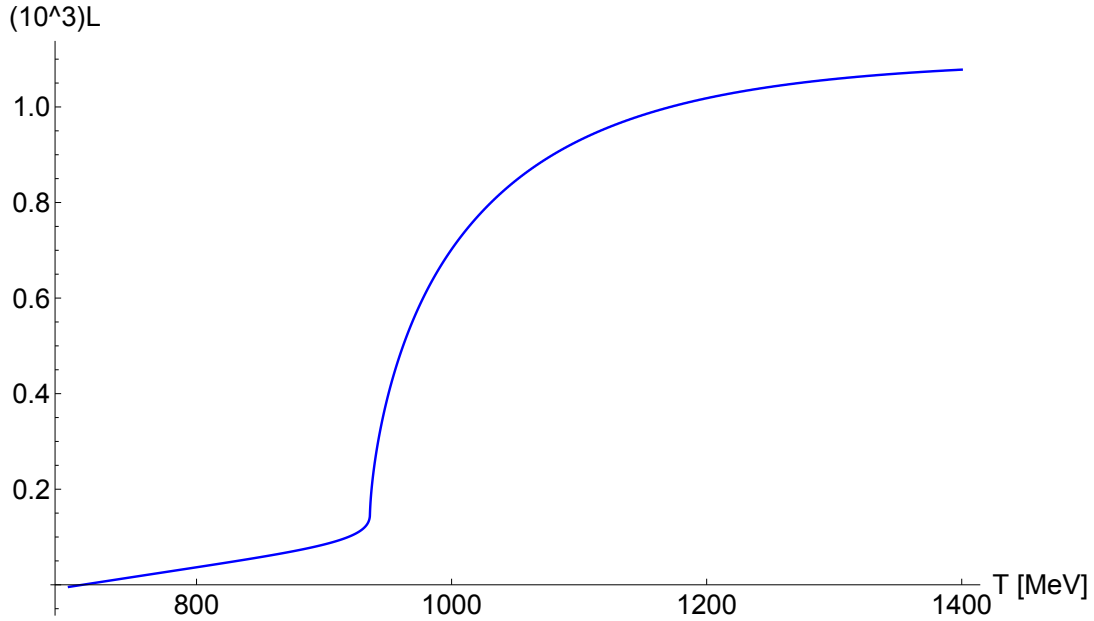


Figure 1.6. The evolution of the lepton number (initially $L_0 = 1.1 \times 10^{-3}$) for $m_s = 64$ keV and $\sin^2 2\theta = 10^{-10}$

Also, due to the dependence on the scaled momentum $x = p/T$, different modes go through the resonance at different temperatures. Thus, resonantly produced sterile neutrinos have a significantly distorted “colder” spectrum compared to the equilibrium Fermi-Dirac distribution. To recap, a massive sterile neutrino is a viable dark matter candidate and it can be efficiently produced in the early universe via mixing with the other regular neutrinos. If sterile neutrinos were in thermal equilibrium until $T \sim 1$ MeV (neutrino decoupling) and retained their Fermi-Dirac spectra then their present number density would be 112 cm^{-3} . This means that keV range thermal neutrinos would significantly exceed the critical density of the Universe (imply a closed rather than a flat Universe). Thus, a keV sterile neutrino must be created non-thermally. In that case they behave as a mixture of “cold” and “warm” dark matter and are compatible with all present observations. Additionally, they are warm enough to “explain” the suppression of small structures in Milky-Way-size galaxies [3].

Figure 1.5 shows state of the art sterile neutrino spectra for sterile neutrino masses m_s and mixing angles θ which satisfy all current observational constraints.

The quantum kinetic equations are a difficult to solve and the Zeno approximation, which recasts the problem in terms of statistical distribution functions rather than quantum amplitudes vastly eases the computational demands and cuts the computational time from days to seconds. Although the QKEs are the more physical approach the Zeno approximation is more popular, and its popularity is justifiable on the grounds of efficacy as well as speed.

Figure 1.7 shows the percent difference between the two methods for the calculation of the sterile neutrino conversion rate df/dT for scaled momentum $x = 1$. The discrepancy is primarily $\sim 0.1\%$ and at most $\sim 1\%$.

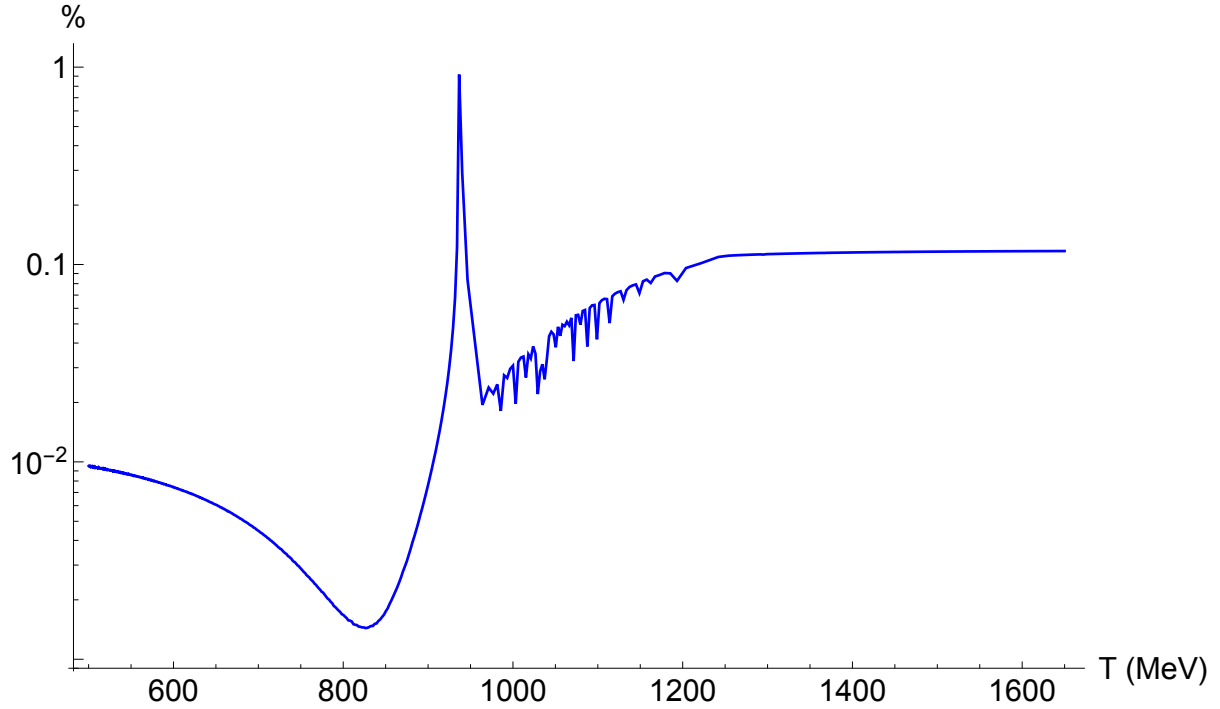


Figure 1.7. Percent difference between the sterile neutrino conversion rate df/dT for scaled momentum $x = 1$ between the Zeno equations and the QKEs. Both systems of equations are for an evolving lepton number (initially $L_0 = 1.1 \times 10^{-3}$) and $m_s = 64$ keV and $\sin^2 2\theta = 10^{-10}$. The jagged behavior is due to the interpolation method used compare the two solutions.

CHAPTER 2

MY RESEARCH

2.1 NUMERICAL METHODS

The QKEs are a prodigious set of coupled, non-linear, differential equations and can take days to solve on a modern laptop. The reason is that the evolution happens on a scattering time scale. Recasting time to temperature this corresponds to roughly 10^{-3} eV. Therefore, to track a decrease in temperature of few GeV requires trillions of steps.

To minimize the number of steps, we sought to maximize the step size and employed an 11 step Runge-Kutta method of the following layout [14].

$$\begin{aligned}
 k_1 &= f(t_n, y_n) \\
 k_2 &= f(t_n + C_2 h, y_n + h(a_{21} k_1)) \\
 k_3 &= f(t_n + C_3 h, y_n + h(a_{31} k_1 + a_{32} k_2)) \\
 &\vdots \\
 k_s &= f(t_n + C_s h, y_n + h(a_{s,1} k_1 + a_{s,2} k_2 + \cdots + a_{s,s-1} k_{s-1})) \\
 y_{n+1} &= y_n + h \sum_{i=1}^s b_i k_i
 \end{aligned}$$

The coefficients $a_{i,j}$ compose a matrix, and b_i and C_i are the "weights" (or nodes). Often, this is visualized using a "Butcher Table."

0					
C_2	a_{21}				
C_3	a_{31}	a_{32}			
\vdots					
C_s	$a_{s,1}$	$a_{s,2}$	\dots	$a_{s,s-1}$	
	b_1	b_2	\dots	b_{s-1}	b_s

A higher order Runge-Kutta method allows for a larger step size because it uses a Taylor series approximation of the solution to find the "weights" that decrease the truncation error at each step. However, the benefit of a larger step size comes at the cost of more

evaluations per step. As a comparison, the classic 4th Order RK method has the following layout.

0				
1/2	1/2			
1/2	0	1/2		
1	0	0	1	
	1/6	1/3	1/3	1/6

The Hamiltonian in the QKEs depends on the lepton number which we did not solve for using this numerical method. Its evolution requires the knowledge of the neutrino spectrum at all temperatures. We implemented the method outlined above to evolve only a *single* scaled momentum x rather than all the momenta. Tracking all the momentum bins, or at least a few hundred, would take a much longer time. Therefore, we used the Zeno result for $L(T)$ in order to solve the QKEs.

2.2 SOLUTIONS TO THE QKES

To study the behavior of the quantum kinetic equations, we evolved a 2×2 neutrino system that includes coupling between ν_e and ν_s in the early universe with an initial lepton asymmetry. We began the evolution at $T = 2$ GeV where due to a small value of $\sin^2 2\theta_M$ we expect nearly zero sterile neutrinos. For comparison with [24], we chose a sterile neutrino of mass $m_s = 64$ keV and mixing angle $\sin^2 2\theta = 10^{-10}$, and assumed an initial lepton number of $L_0 = 1.1 \times 10^{-3}$ in each ν flavor. Although these parameters do not obey the current x-ray bounds, they nonetheless offer some important insights.

Figure 2.1 shows the solutions to the QKEs for a constant lepton asymmetry and an initial temperature $T_0 = 1.65$ GeV for a sterile neutrino of scaled momentum $x \equiv p/T = 1$. The initial condition is on the right and time increases to the left. The top left plot is $10^4 \times P_x$ and the top right plot is $-10^4 \times P_y$. We rescaled the y axis in order to emphasize the miniscule amount of coherences built up in this high scattering environment. Because the evolution of the ν states is most interesting around the resonances, we only show the evolution up to $T = 0.5$ GeV, or just past the second resonance. As discussed in Section 1.11, for keV mass range sterile neutrinos there are two resonances in the production because at high temperature the second term in the forward scattering potential dominates and at lower temperature the first term dominates. The two middle plots in Figure 2.1 show P_0 , which is

proportional to the total number of both neutrino species, and P_z , which starts at 1 (corresponding to no sterile neutrinos) and decreases with temperature. As P_z decreases, more electron neutrinos convert to sterile neutrinos. The bottom part of Figure 2.1 shows the two peaks in the sterile neutrino production rate, for a scaled momentum of $x = 1$. In terms of the polarization vector, this rate is

$$\frac{df}{dT} = \frac{1}{2} \left(\frac{dP_0}{dT} - \frac{dP_0}{dT} P_z - P_0 \frac{dP_z}{dT} \right) \quad (2.1)$$

The peaks in the conversion rate seem more pronounced than the dips in P_z and elevations in P_0 because we plot df/dT on a log scale.

Although, the case of a constant lepton asymmetry is unphysical, for reasons discussed in Section 1.11, it illustrates a key quantum kinetic effect. The coherent and decoherent terms in the equations of motion balance each other, or “equilibrate.” This is evident from the top two plots in Figure 2.1. P_x and P_y barely change even at resonances. In other words, coherences have little time to build up between decoherent scatterings. This is *the* reason why the Zeno approximation works.

We show the solutions to the QKEs for the more physical case of an evolving lepton number in Figure 2.2. Simply by glancing at Figure 2.1 and Figure 2.2 side by side one can spot the crucial similarities between the two approaches. First of all, both for a constant and a changing lepton number, there are two resonances in the sterile neutrino production rate, although for an evolving lepton asymmetry the temperature of these resonances change. Secondly, in both cases coherences barely build up. We dub this phenomenon as “quantum kinetic equilibration” and discuss it in more detail in Section 2.3. As electron neutrinos are converted to sterile neutrinos, L decreases and, in turn, a shrinking L accelerates the MWS resonance sweep rate. This feedback lasts as long as there are MSW resonances and quickly reduces the lepton number (shown in the bottom left portion of Figure 2.2).

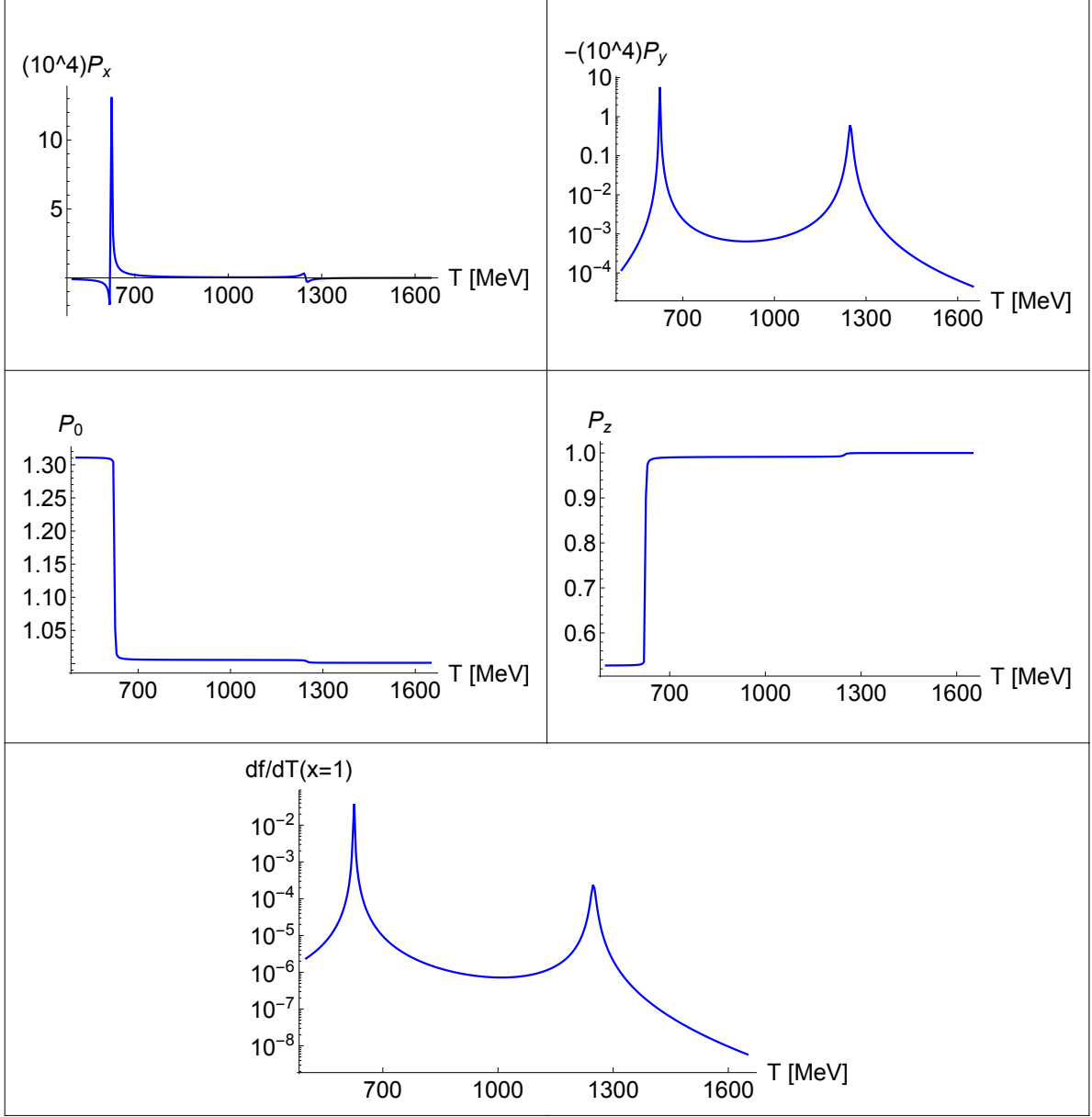


Figure 2.1. Solutions to the QKEs for a constant lepton number $L = 1.1 \times 10^{-3}$ ($m_s = 64$ keV, $\sin^2 2\theta = 10^{-10}$). The top two panels show $10^4 P_x$ and $-10^4 P_y$ vs. T , the middle two panels show P_0 and P_z vs. T , and the bottom panel shows the sterile neutrino conversion rate df/dT for $x = 1$.

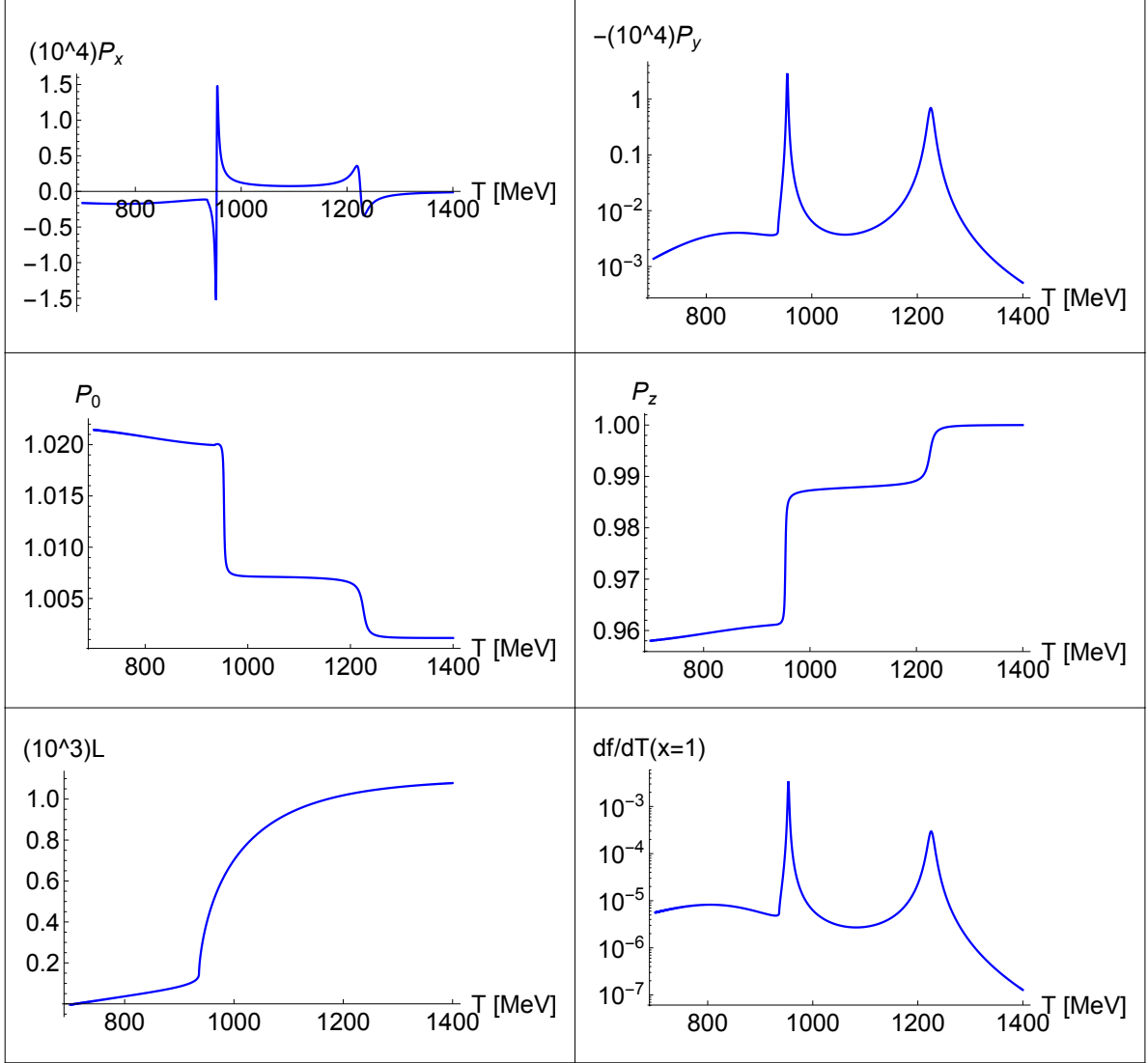


Figure 2.2. Solutions to the QKEs for an evolving lepton number L . Initially, $L_0 = 1.1 \times 10^{-3}$. As for the constant lepton number case, $m_s = 64$ keV and $\sin^2 2\theta = 10^{-10}$. The top two panels show $10^4 P_x$ and $-10^4 P_y$ vs. T and the middle two panels show P_0 and P_z vs. T . The bottom left panel shows the evolution of L and the bottom right panel shows the sterile neutrino conversion rate df/dT for $x = 1$.

Evolving a rapidly varying quantum amplitude, as done in the QKEs, is much more computationally intensive than evolving statistical distribution functions, as done in the Zeno approximation. Therefore, we do not plot a sterile neutrino spectrum, which would require tracking neutrinos of many different scaled momenta $x = p/T$ to self consistently evolve the lepton number along with the $\nu_e \leftrightarrow \nu_s$ conversion. Even the evolution of a *single* x takes roughly a day on a modern laptop. On the other hand, the Zeno approximation can generate a spectrum (or a phase space density) in a matter of seconds.

2.3 QUANTUM KINETIC EQUILIBRIUM

Since the oscillation frequency ω responsible for the growth of coherences and the decoherent scattering rate Γ responsible for the damping of such coherences are both fast compared to the expansion rate of the Universe, we expect some sort of “equilibrium” between these opposing processes. Figure 2.3 shows both frequencies in units of inverse temperature. The time increases to the left.

By “equilibrium” we do *not* mean that the two frequencies are the same. Instead, we mean that since the background Universe expands at a rate slower than ω and Γ , the evolution proceeds from one local thermal equilibrium to another as dictated by ω and Γ .

This balance practically fixes P_x and P_y allowing us to find their analytic, equilibrium form. Setting $\dot{P}_x \approx \dot{P}_y \approx 0$ gives

$$P_x = \frac{P_0^2 P_z V_x V_z}{(P_0 V_z)^2 + (\dot{P}_0 + P_0 \mathcal{D})^2} \quad (2.2)$$

$$P_y = -\frac{P_0 P_z V_x (\dot{P}_0 + P_0 \mathcal{D})}{(P_0 V_z)^2 + (\dot{P}_0 + P_0 \mathcal{D})^2} \quad (2.3)$$

To illustrate, that this idea does indeed work, we plot the difference between the full solutions to the quantum kinetic equations and their equilibrium form. Figure 2.4 shows one minus the absolute value of the ratio of the equilibrium values of P_x and P_y to the full values of P_x and P_y determined from a complete solution to the QKEs.

The equilibrium P_x and P_y depend on the evolution P_0 and P_z . Instead of consistently evolving the whole equilibrium system of equations, we plucked P_0 and P_z from the full solution of the QKEs and plugged it into the analytical forms of \mathbf{P}_\perp . In this case, the discrepancies are $\ll 10^{-5}$.

At the resonances the coherent and decoherent terms in the equations of motion are not exactly balanced and the equilibrium equations deviate the most from the full solutions. A further discussion of this point is given in the next section.

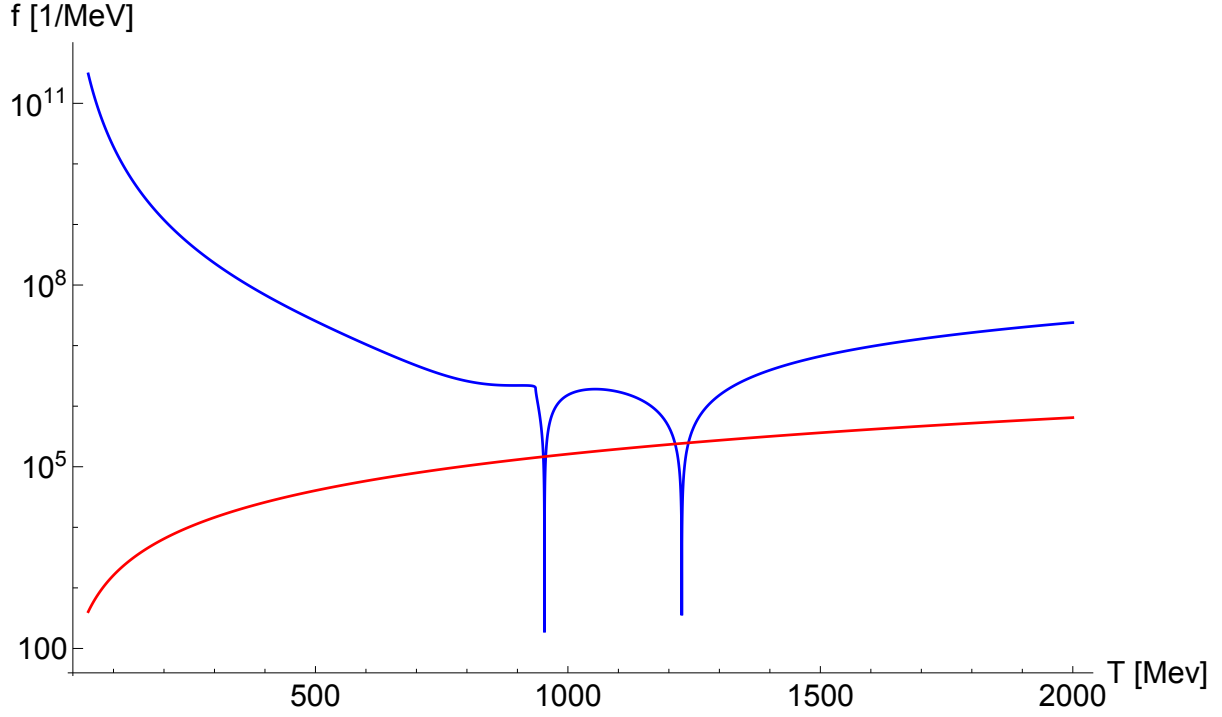


Figure 2.3. The oscillation frequency ω (blue) and the scattering frequency Γ (red) in units of inverse MeV vs. temperature. The time increases to the left.

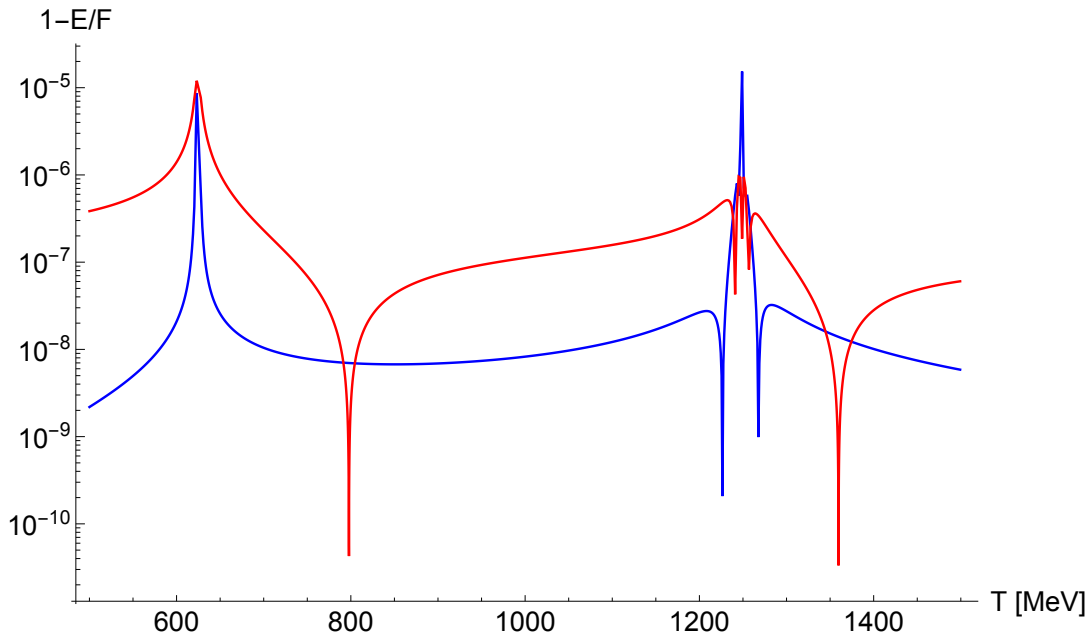


Figure 2.4. $(1 - \text{Abs}(E/F))$ vs. T for a constant lepton number, where E corresponds to the equilibrium values of P_x (blue) and P_y (red) and F to the full values. The equilibrium P_x and P_y depend on P_0 and P_z , which we took from the full solutions to the QKEs.

In essence, the quantum kinetic equilibrium halves the computational demands. Using the analytic value of \mathbf{P}_\perp , we only have to numerically solve for P_z and P_0 . Explicitly, the equations of motion become

$$P_x = \frac{P_0^2 P_z V_x V_z}{(P_0 V_z)^2 + (\dot{P}_0 + P_0 \mathcal{D})^2} \quad (2.4)$$

$$P_y = -\frac{P_0 P_z V_x (\dot{P}_0 + P_0 \mathcal{D})}{(P_0 V_z)^2 + (\dot{P}_0 + P_0 \mathcal{D})^2} \quad (2.5)$$

$$\dot{P}_z = V_x P_y + (1 - P_z) \dot{P}_0 / P_0 \quad (2.6)$$

$$\dot{P}_0 = \Gamma \left(\frac{e^x + 1}{e^{x-\eta} + 1} - \frac{P_0}{2} (1 + P_z) \right). \quad (2.7)$$

Figure 2.5 compares the solutions to these equilibrium equations to the solutions from the full quantum kinetic equations. Just as Figure 2.4, Figure 2.5 shows one minus the absolute value of the ratio of the equilibrium values of P_x and P_y to the full QKE solutions of P_x and P_y . Except now, instead of plugging in the actual values of P_0 and P_z into the equilibrium equations, P_0 and P_z are evolved independently using the equilibrium values of P_x and P_y . As before, the equilibrium values never deviate from the actual values by more than 10^{-5} .

At temperatures much higher than the resonances, we expect to have zero sterile neutrinos. In other words, $\dot{P}_0 \approx 0$. Paired with the equilibrium condition, this extra piece of physics allows to make another useful approximation for P_x and P_y . Namely,

$$P_x = \frac{\omega^2 \sin 2\theta_M}{(\omega^2 + (\Gamma/2)^2)} \quad P_y = -\frac{\omega \sin 2\theta_M \Gamma}{2(\omega^2 + (\Gamma/2)^2)}. \quad (2.8)$$

In these equations, $V_x/|\mathbf{V}| = \sin 2\theta_M$ and $|\mathbf{V}| = \omega \approx V_z$ and $P_z = 1$. For temperatures above 2 GeV, P_x and P_y have a simple dependence on T. For instance, $P_x \approx (2 \times 10^{12}) T^{-6}$.

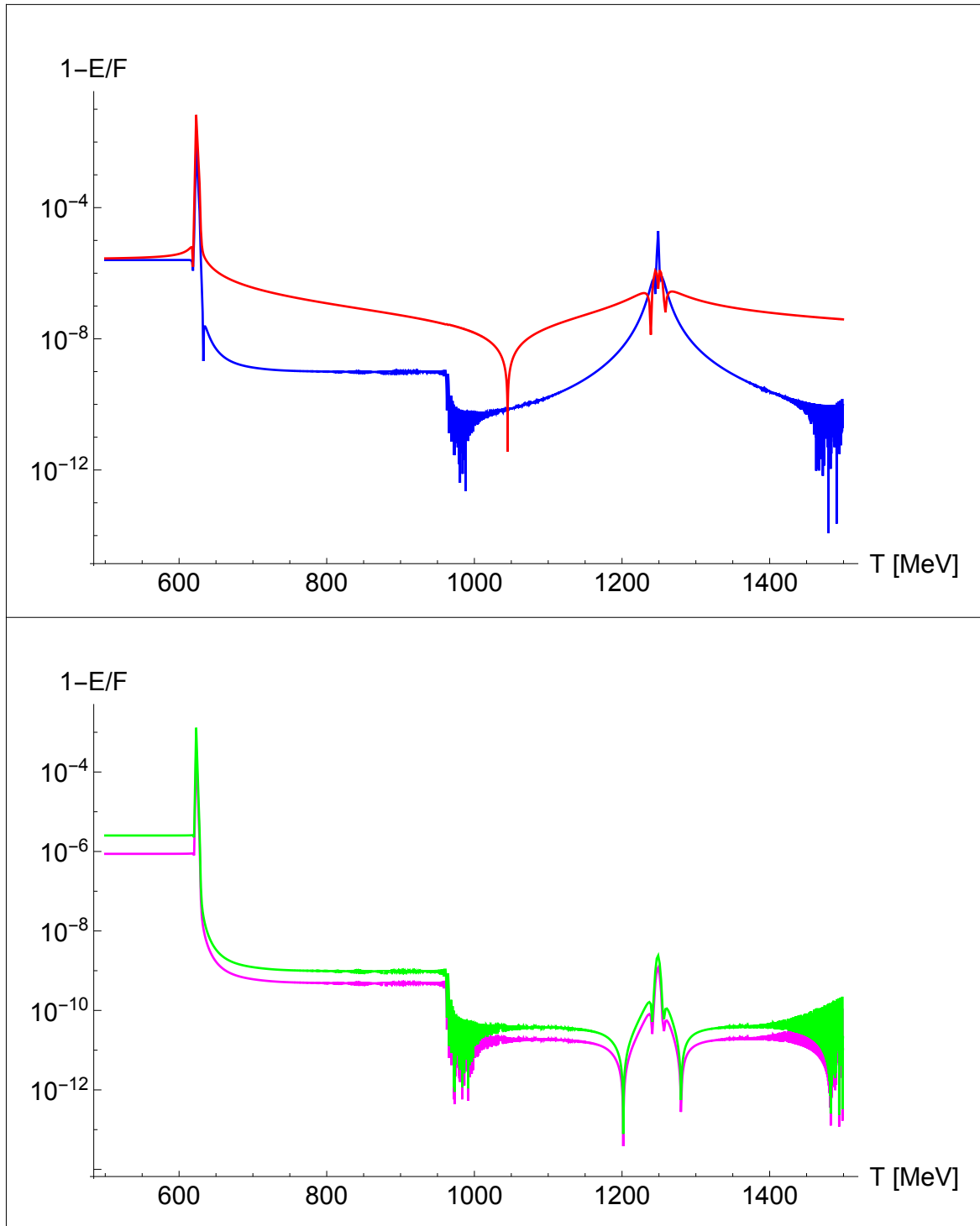


Figure 2.5. $(1 - \text{Abs}(E/F))$ vs. T for a constant lepton number, where E corresponds to the equilibrium solutions and F to the full solutions. The comparison is blue for P_x and red for P_y (top box), and magenta for P_0 and green for P_z (bottom box).

2.4 THE GEOMETRY OF THE QKES AT RESONANCES

Above $T \sim 500$ MeV, neutrinos are still coupled and immersed in a plasma in which they experience forward scattering and decoherent scattering. The entropy of the plasma at this epoch is stored in e^\pm , μ^\pm , and neutrinos. We consider the mixing of two flavors, the electron and sterile neutrinos, and evolve a 2×2 density matrix which has the following form in a Pauli basis

$$\rho = \frac{1}{2}P_0(\mathbb{1} + \mathbf{P} \cdot \boldsymbol{\sigma}). \quad (2.9)$$

The off-diagonal entries measure coherence between the two flavors and the diagonal entries indicate the individual flavor densities. The diagonal elements are

$$\rho_{\alpha\alpha} = \frac{1}{2}P_0(1 + P_z) \quad (2.10)$$

$$\rho_{ss} = \frac{1}{2}P_0(1 - P_z) \quad (2.11)$$

where P_0 is a normalization factor proportional to the total number of active and sterile neutrinos with scaled momentum $x = p/T$. $P_z = -1$ means that all the neutrinos are sterile, $-1 < P_z < 1$ that there is a mixture of both flavors, and $P_z = 0$ that there is an equal number of both. The equations of motion for density matrix ρ are

$$i\dot{\rho} = [\mathcal{H}, \rho] + \mathcal{C} \quad (2.12)$$

where \mathcal{H} is the Hamiltonian operator that accounts for coherent evolution and \mathcal{C} is the collision operator that comes from the evaluation of Boltzmann integrals and accounts for decoherent scattering. Collisions destroy coherence and possibly change the neutrino momentum and/or flavor. In terms of the polarization vector \mathbf{P} these equations are

$$\dot{\mathbf{P}} = \mathbf{V} \times \mathbf{P} + (1 - P_z)(\dot{P}_0/P_0)\hat{z} - (\mathcal{D} + (\dot{P}_0/P_0))\mathbf{P}_\perp \quad (2.13)$$

$$\dot{P}_0 = \Gamma \left(\frac{e^x + 1}{e^{x-\eta} + 1} - \frac{1}{2}P_0(1 + P_z) \right) \quad (2.14)$$

\dot{P}_0 keeps ν_e in thermal equilibrium with the plasma, and $\mathbf{P}_\perp = P_x\hat{x} + P_y\hat{y}$. The decoherence function \mathcal{D} encodes the weak interaction scattering amplitudes of the neutrino flavors and it is a common assumption that $\mathcal{D} = \Gamma/2$ [31].

At high temperature, coherences do not develop and \mathbf{P} sits at a local equilibrium value near \mathbf{V} - the Hamiltonian responsible for the coherent evolution (both vacuum oscillations and matter induced forward scattering). \mathbf{V} is a parametrization of \mathcal{H} in a Pauli basis and encodes

the same physics. Just because the phase does not build up does not mean that P_x and P_y are zero. There *are* coherences. This is Zeno's Paradox at play. As the temperature decreases, \mathbf{P} traverses a path dictated by the quantum kinetic equilibrium. The Hamiltonian \mathbf{V} also evolves with changing temperature and shepherds \mathbf{P} along, and the degree to which \mathbf{P} can follow \mathbf{V} is a function of adiabaticity.

As expected, the neutrino flavor evolution depends on two time scales; the scattering time and the oscillation time. Initially, before the second resonance, V_z points up and then swings down. This is simply due to the changing density in an expanding universe. Explicitly,

$$V_z = \left(\frac{2\sqrt{2}\zeta(3)}{\pi^2} G_F \mathcal{L}_e T^3 - r_e G_F^2 x T^5 \right) - \frac{\delta m^2 \cos 2\theta}{2xT} \quad (2.15)$$

and

$$V_x = \frac{\delta m^2 \sin 2\theta}{2xT} \quad (2.16)$$

where

$$\mathcal{L}_e \equiv 2L_e + \sum_{\beta \neq e} L_\beta \quad (2.17)$$

is the potential lepton number depending on neutrino, antineutrino and photon number densities. As the universe cools, V_z resonantly changes sign from positive to negative. The first term in V_z corresponds to forward scattering and the second term to vacuum oscillations. Note, V_x is only due to vacuum oscillations and does not change sign. Therefore, a flip in V_z means that the oscillation term and the forward scattering terms become equal.

When the change is adiabatic \mathbf{V} shepherds \mathbf{P} along: the angle between \mathbf{V} and \mathbf{P} is small. However, the resonances in the early universe, during which V_z quickly changes sign, are anything but adiabatic. Initially \mathbf{P} follows \mathbf{V} but immediately after \mathbf{V} 's sudden flip the leash is broken and \mathbf{P} cannot follow along and slowly migrates away from its pre-resonance position to a new local equilibrium. Figure 2.6 shows just how close \mathbf{P} lies to \mathbf{V} in the adiabatic regime and how little \mathbf{P} shifts after \mathbf{V}_z resonantly changes sign. The top right panel is $\sin^2 \theta$ where θ is the angle between \mathbf{V} and \mathbf{P} . This angle is either really close to 0 or π . Therefore, $\sin^2 \theta$ is negligible when subtracted from $\sin^2 \theta_M$ (bottom right panel). The bottom left panel shows $\sin^2 \theta_M$ by itself. The top left panel shows $\cos \theta$ and illustrates just how quickly the angle between \mathbf{V} and \mathbf{P} changes from nearly 0 to nearly π when V_z changes sign.

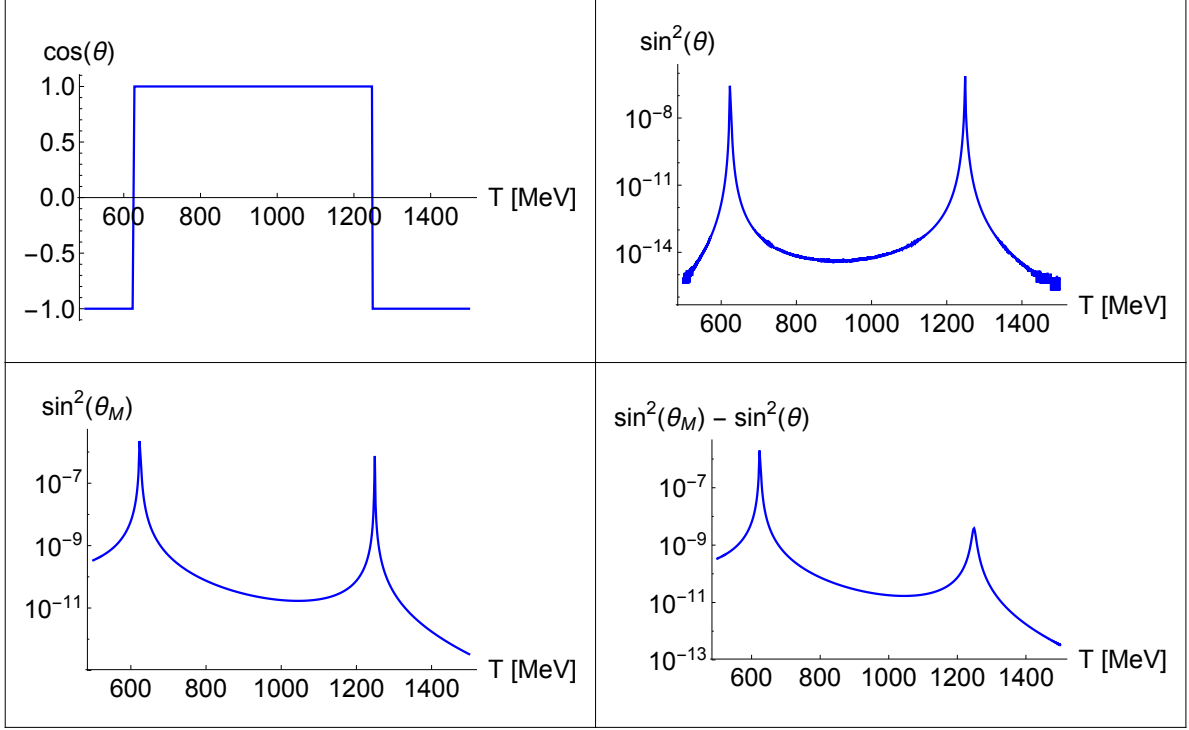


Figure 2.6. The top left panel is $\cos \theta$ where θ is the angle between \mathbf{V} and \mathbf{P} . The top right panel is $\sin^2 \theta$. The bottom left panel is $\sin^2 \theta_M$ where θ_M is the in medium mixing angle. The bottom right panel is the difference of $\sin^2 \theta_M$ and $\sin^2 \theta$. These figures are for a constant lepton number.

Furthermore, V_z changes sign when the coherent term in the equations of motion becomes larger than the decoherent term. As this happens, \mathbf{P} traces out an arc and P_x switches sign from positive to negative. Also, the quantum kinetic equilibrium dictates that $P_x = 0$ when $V_z = 0$. Figure 2.7 shows this resonant behavior by plotting the unit projection of \mathbf{P} in the x, y plane and \mathbf{V} in the x, z plane. Points 1, 2, and 3 correspond to progressively decreasing temperature and increasing time.

The bottom portion of Figure 2.7 shows the unit projection of the cross product $\mathbf{V} \times \mathbf{P}$ in the x, y plane. This is the coherent term which becomes larger at resonance. It is clear from Figure 2.7 that there is no "equilibration" at the resonance. This is because the scattering time scale is larger than the oscillation time scale. "Equilibration" only applies when the scattering time scale is much smaller than the oscillation time scale. In fact, it is the fact that $\dot{P}_x \neq 0$ and $\dot{P}_y \neq 0$ that is responsible for these arcs. However, $\dot{P}_x \approx \dot{P}_y \approx 0$ is still a good approximation even the resonances because \dot{P}_x and \dot{P}_y are still small compared to the scattering rate.

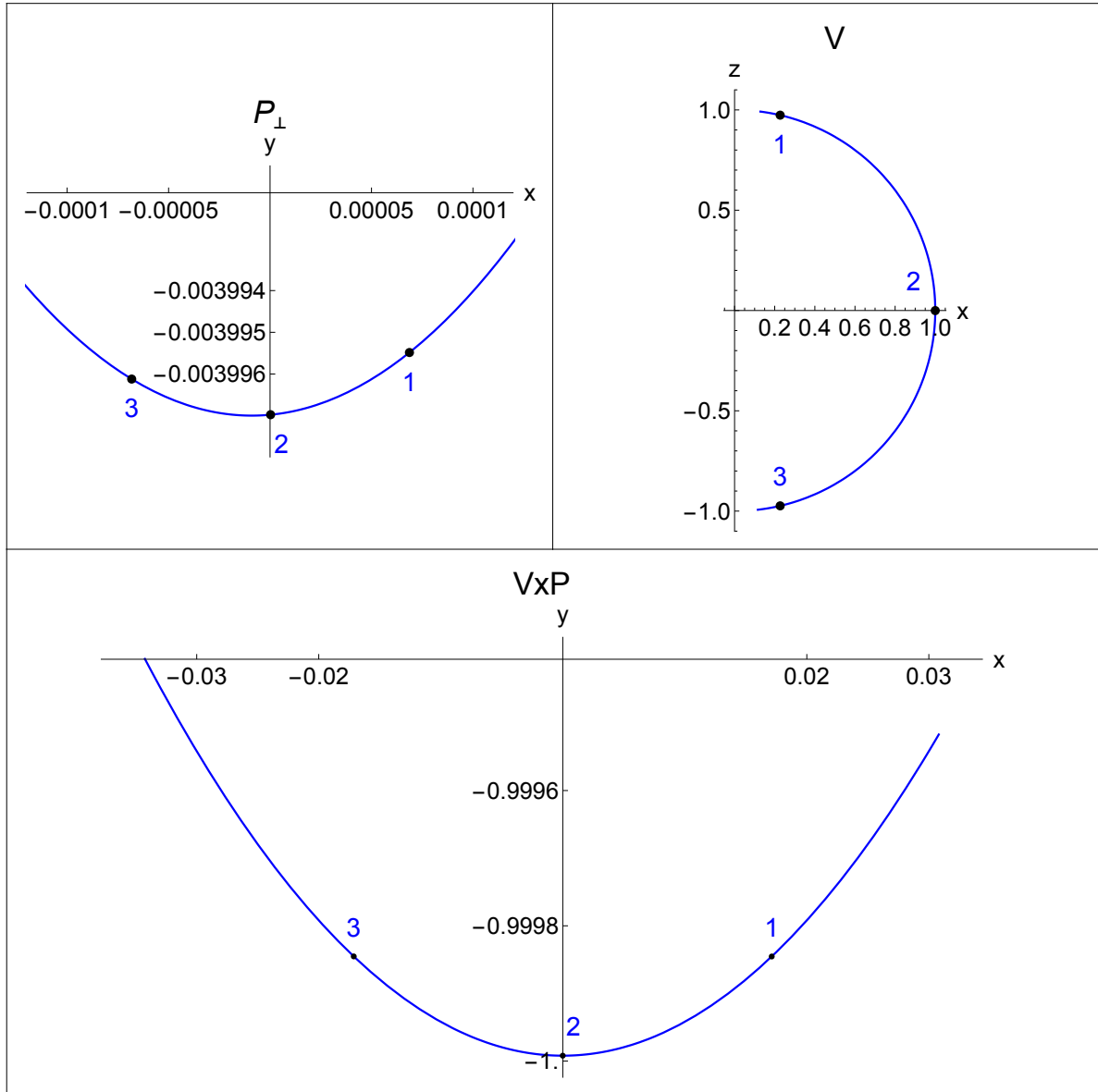


Figure 2.7. Constant lepton number evolution of the unit projections of \mathbf{P} (top left), \mathbf{V} (top right), and $\mathbf{V} \times \mathbf{P}$ (bottom) through a resonance. Points 1,2, and 3 correspond to progressively decreasing temperatures of $T = 624.385$ MeV, $T = 624.377$ MeV, and $T = 624.369$ MeV, or alternatively, increasing time. The resonance happens at Point 2.

Figure 2.8 shows the projections of \mathbf{P} , \mathbf{V} and $\mathbf{V} \times \mathbf{P}$ for the case of an evolving lepton number. P_x is still zero when $V_z = 0$ but because of a changing lepton number the resonance happens at a different temperature $T = 953.603$ MeV.

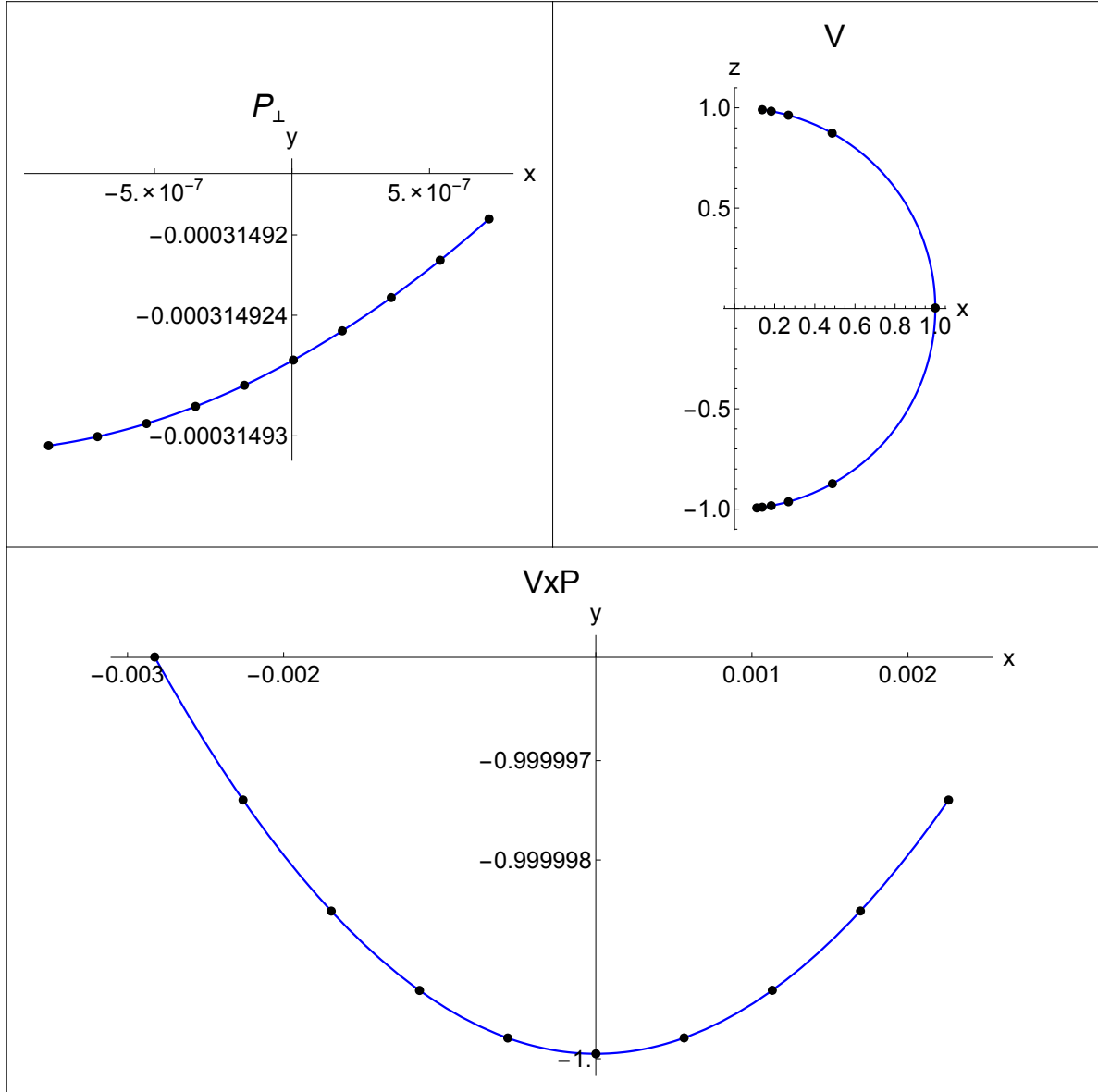


Figure 2.8. Unit projections of \mathbf{P} (top left), \mathbf{V} (top right), and $\mathbf{V} \times \mathbf{P}$ (bottom) through a resonance for the case of an evolving lepton number. Just as in Figure 2.7 the temperature decreases as the arc swings from right to left in the top left and the bottom panels. In the top right panel, the temperature decreases as the arc swings from 1 to -1. The first point corresponds to $T = 953.606$ MeV; the last to $T = 953.600$ MeV. Due to a changing lepton number, the resonance (the point at $x = 0$) happens at a different temperature than in Figure 2.7

2.5 INITIAL CONDITIONS AND “RINGING”

The initial conditions for the quantum kinetic equations, in particular the polarization vector \mathbf{P} , are governed by the fact that the weak interaction scattering Hamiltonian is diagonal in the flavor basis. At high temperatures, nearly all of the neutrinos should be active rather

than sterile since $\sin 2\theta_M$ is extremely small and we expect the polarization vector to be $\mathbf{P} = (0, 0, 1)$. In the literature, this is the commonly used initial condition [24]. In this case, the density operator is

$$\rho = \frac{1}{2}P_0 \begin{pmatrix} 1 + P_z & P_x - iP_y \\ P_x + iP_y & 1 - P_z \end{pmatrix} \approx \begin{pmatrix} P_0 & 0 \\ 0 & 0 \end{pmatrix}. \quad (2.18)$$

However, as shown in Section 2.3, the high temperature equilibrium values are

$$P_x = \frac{\omega^2 \sin 2\theta_M}{(\omega^2 + (\Gamma/2)^2)} \quad P_y = -\frac{\omega \sin 2\theta_M \Gamma}{2(\omega^2 + (\Gamma/2)^2)} \quad P_z = 1. \quad (2.19)$$

Because the commonly used initial \mathbf{P} is inconsistent with the equilibrium, P_x and P_y undergo damped oscillations to attain it. Henceforth, we will refer to these dying oscillations as “ringing.” Figure 2.9 shows this behavior for P_x for a span of 10 eV after an initial temperature of $T = 2$ GeV. In this figure, the temperature decreases to the right. Alternatively, the time increases to the right. The x axis corresponds to the temperature after 2 GeV, or $(2 \text{ GeV} - T)$.

“Ringing” is a numerically convergent phenomenon and smaller step sizes lead to the same result. In other words, it is a relaxation of the dynamical variables to an “equilibrium” value and *not* a numerical artifact or the result of a truncation error. In fact, the ringing is predictable from the parameters in the equations and is extremely well modeled by an underdamped oscillator of oscillation frequency $\omega = |\mathbf{V}|$ and decay frequency $\xi = \mathcal{D} = \Gamma/2$. More explicitly,

$$P_x = P_{x,eq} + (P_{x,0} - P_{x,eq}) e^{-\xi|T-T_0|} \cos(\omega(T - T_0)). \quad (2.20)$$

where $T < T_0$, $P_{x,0}$ is the initial value of P_x , and $P_{x,eq}$ is the equilibrium value of P_x . The model for P_y is exactly the same modulo the ensuing equilibrium value. In other words, P_y has the same oscillation frequency ω and damping frequency ξ but settles to a different equilibrium than P_x . Figure 2.9 shows the underdamped “ringing” for the point at $T = 2$ GeV where the oscillation frequency is given by ω and the damping rate is $\xi = \mathcal{D}$.

Figure 2.10 shows the ω and ξ resulting from initializing \mathbf{P} at $(0, 0, 1)$ at initial temperatures of $T = 1.5$ GeV, $T = 1.8$ GeV and $T = 2$ GeV superimposed over the underdamped oscillator model with $\xi = \mathcal{D}$ and $\omega = |\mathbf{V}|$. As expected, the exponential damping to equilibrium is governed by scattering, hence $\xi = \mathcal{D}$. Also, in the context of the precession analogy provided in Chapter 1, it is not a surprise that the oscillation frequency $\omega = |\mathbf{V}|$.

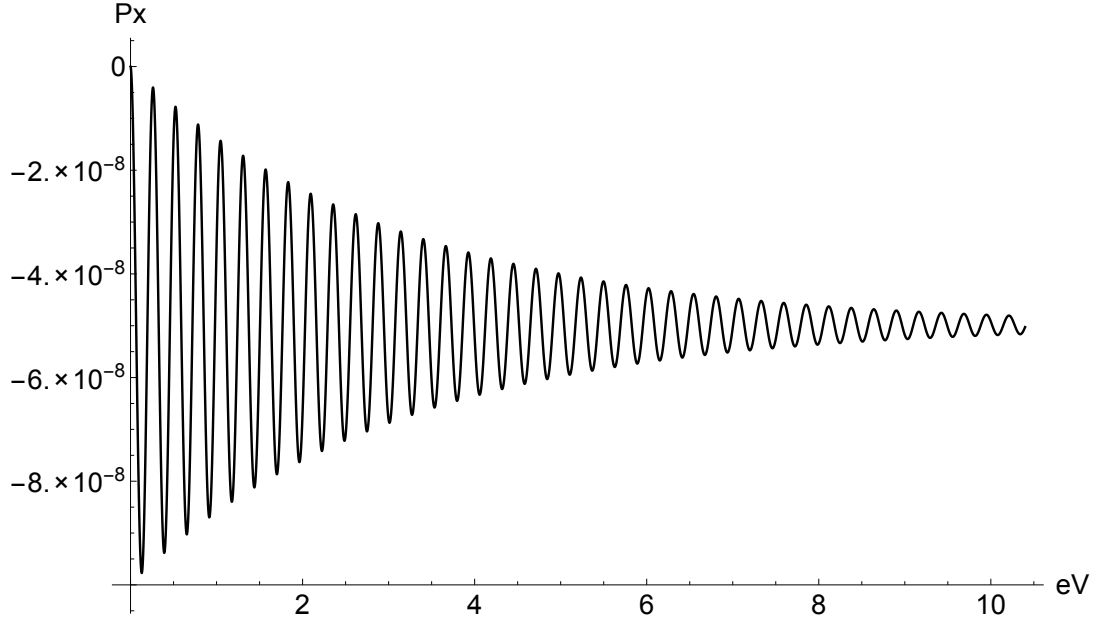


Figure 2.9. Ringing of P_x for a span of 10 eV after 2 GeV. The x axis is $(2 \text{ GeV} - T)$. The time increases to the right. The oscillation frequency is $\omega = |\mathbf{V}| = 2.1 \times 10^{-4} \text{ MeV}^{-1}$ and the damping frequency is $\xi = \mathcal{D} = 2.8 \times 10^{-6} \text{ MeV}^{-1}$. This evolution is for a constant lepton number.

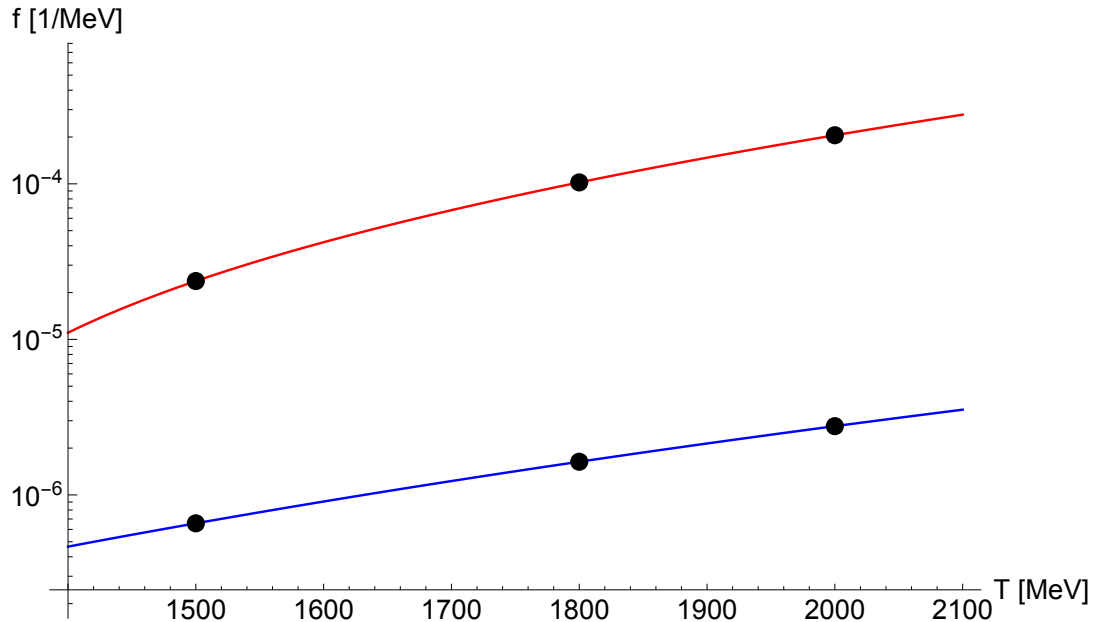


Figure 2.10. The oscillation frequency ω (red) and the damping frequency ξ (blue) in units of $1/\text{MeV}$ vs. temperature (MeV) for a constant lepton number. We chose the bolded points to test the underdamped oscillator model. Figure 2.9 shows the point corresponding to $T = 2000 \text{ MeV}$, where $\omega = 2.1 \times 10^{-4} \text{ MeV}^{-1}$ and $\xi = \mathcal{D} = 2.8 \times 10^{-6} \text{ MeV}^{-1}$.

The ringing happens at all temperatures, is very short lived, and always funnels to the local thermal equilibrium values. Additionally, the ringing takes the same form regardless of the choice of the initial polarization vector \mathbf{P} . Figure 2.11 shows the ringing of two initial values of P_x : 0 and -2.5×10^{-8} . Both evolutions have the same ξ and ω and settle to the same equilibrium value. Again, this is due to high scattering.

Figure 2.12 shows the ringing of P_x for larger step sizes which *do* suffer from truncation errors and therefore lead to unphysical ringing which appears to depend on the step size. However, even these large iteration steps reach the same equilibrium as the smaller steps. Therefore, even though the ringing behavior differs for small and large iteration steps, we can use a large step. The relevant time scales in determining the correct step size are ultimately ω and Γ , not the ringing. The ringing has no effect on the overall results and if we use the proper equilibrium values as the initial conditions then it does not happen.

Finally, we omitted discussing an evolving lepton number because the conclusions for a changing lepton number are the same. This is because at high temperature, $P_z \approx 1$ and does not change.

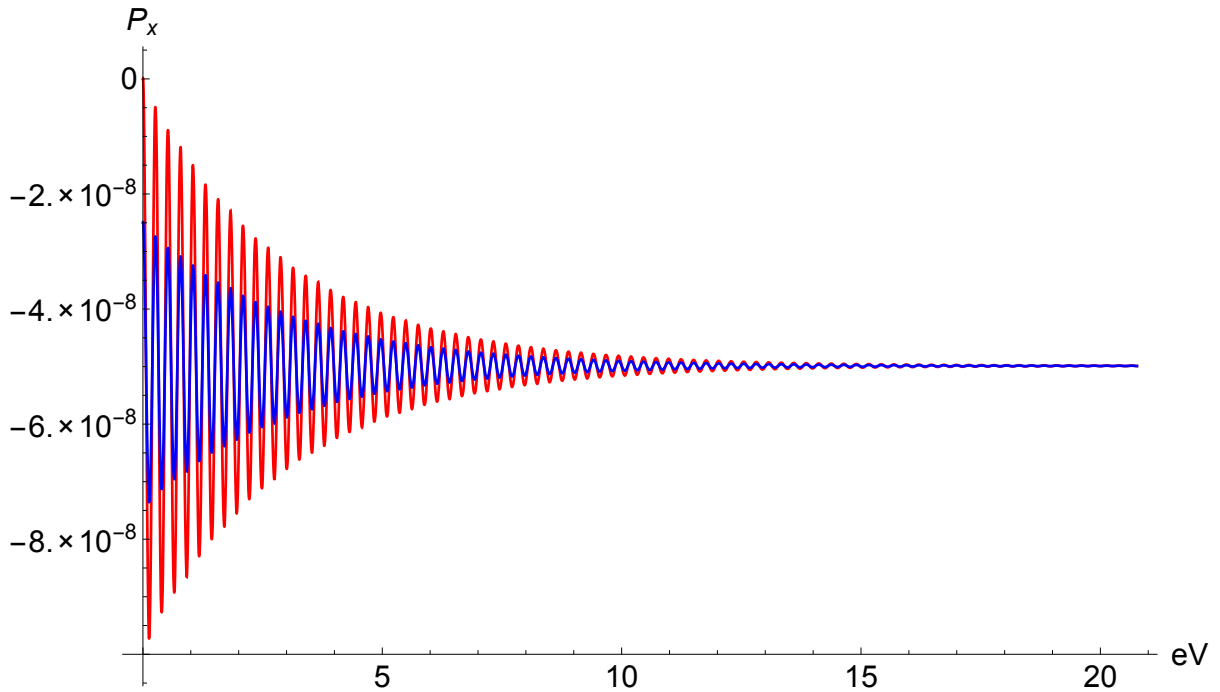


Figure 2.11. Two initial values of P_x relaxing to the same equilibrium point with the same oscillation frequency ω and damping frequency ξ . The plot shows a span of 20 eV after 2 GeV. The x axis is $(2 \text{ GeV} - T)$. The temperature decreases to the right and the time increases to the right.

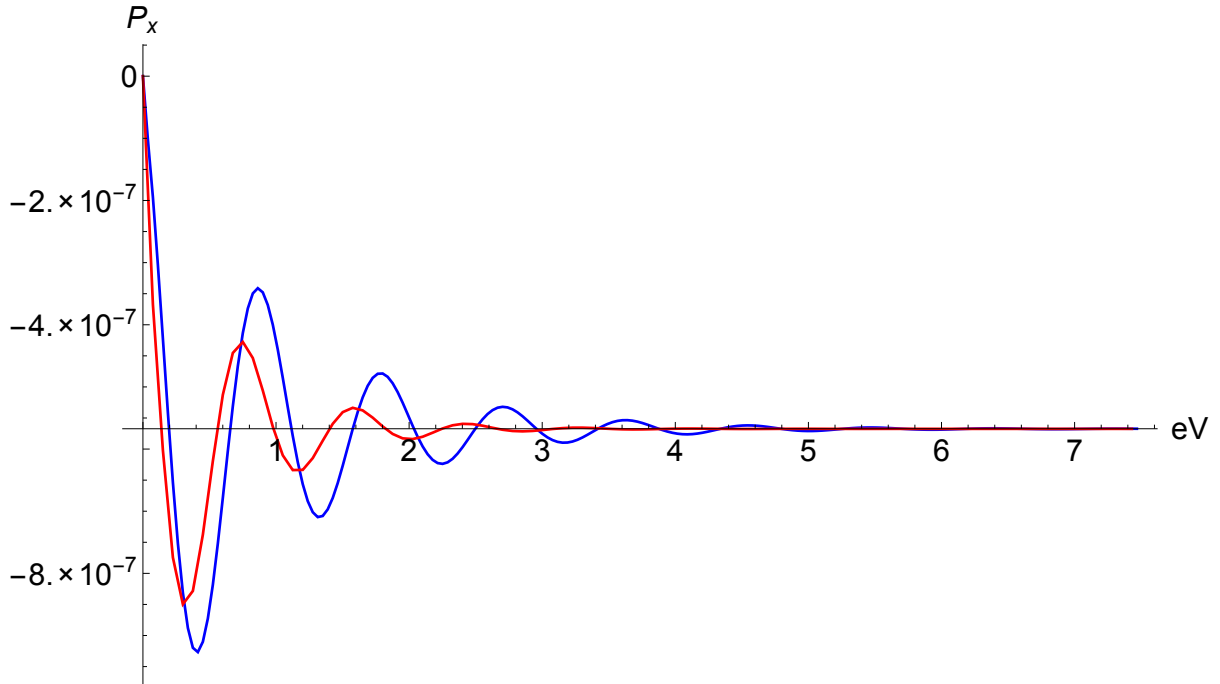


Figure 2.12. P_x for different step sizes. The blue lines corresponds to $dT = 3.8 \times 10^{-2}$ eV and the red line corresponds to $dT = 7.5 \times 10^{-2}$ eV. The plot shows a span of 7 eV after 1.5 GeV. The x axis is $(1.5 \text{ GeV} - T)$. The temperature decreases to the right and the time increases to the right. Each step size settles to the same equilibrium.

CHAPTER 3

CONCLUSION

A recent detection of an anomalous 3.5 keV x-ray line in structures which harbor large amounts of dark matter has revitalized interest in sterile neutrino dark matter. We applied the quantum kinetic equations to the evolution of neutrinos in the early universe with a lepton asymmetry and studied the behavior of the resonant conversion of electron-to-sterile neutrinos. Even at non adiabatic resonances, we found a balance, or a “quantum kinetic equilibrium,” of the growth of coherences and their damping through scattering.

This equilibrium is a useful guide for selecting the proper initial conditions for evolving neutrino states in the early universe. Also, it halves the computational demands of the quantum kinetic equations.

Understanding the evolution of sterile neutrino dark matter in the early universe is important. Although the Standard Model of particle physics is extremely successful, it does not explain neutrino oscillations, dark matter, or the cosmological baryon asymmetry. And it is astounding that these issues can be remedied by simply including sterile neutrinos [7, 8, 15, 19].

Dark matter interactions with ordinary matter are yet to be observed. Therefore, understanding the signatures of potential dark matter candidates is crucial. Different models of dark matter predict different observable effects. In particular, the production mechanism for dark matter and also the distribution of dark matter shape how nucleosynthesis works and how large scale structures form [20, 25, 26]. The existence of a sterile neutrino which mixes with active neutrinos can change fundamentally the relationship between the cosmological lepton numbers and the primordial nucleosynthesis ^4He yield [1]. Also, sterile neutrinos could explain the suppression in the formation of small-scale structures and be in accord with Local Group and high z galaxy count constraints [3].

Additionally, sterile neutrinos are not just of interest to cosmologists. After all, knowing how neutrinos behave and potentially oscillate into yet undiscovered flavors in a high density medium is very applicable to supernovae which release the majority of their gravitational binding energy in neutrinos. The presence of sterile neutrinos can enhance the electron neutrino luminosity by 10% to 100% during the crucial shock reheating epoch [21]. Also, sterile neutrino transport-enhanced entropy deposition ahead of the shock can melt heavy nuclei and reduce the nuclear photo-dissociation burden of the shock and increase the chance of a successful core collapse explosion.

Physicists hoped that the Hitomi satellite, launched last year, could resolve the width of the 3.5 keV line to determine whether it originates from dark matter particles or atomic transitions and whether the flux of the line weakens at the edges of galaxy clusters as predicted for dark matter [5]. Unfortunately, Hitomi malfunctioned before collecting enough data and we have to wait until the 2020s for another mission of equal sensitivity. For now, the sterile neutrino dark matter remains an intriguing speculation.

BIBLIOGRAPHY

- [1] K. ABAZAJIAN, N. F. BELL, G. M. FULLER, AND Y. Y. Y. WONG, *Cosmological lepton asymmetry, primordial nucleosynthesis and sterile neutrinos*, Phys. Rev. D, 72 (2005), p. 063004.
- [2] K. ABAZAJIAN, G. M. FULLER, AND M. PATEL, *Sterile neutrino hot, warm, and cold dark matter*, Phys. Rev. D, 64 (2001), p. 023501.
- [3] K. N. ABAZAJIAN, *Resonantly produced 7 kev sterile neutrino dark matter models and the properties of milky way satellites*, Phys. Rev. Lett., 112 (2014), p. 161303.
- [4] P. ADE ET AL., *Planck 2015 results-xiii. cosmological parameters*, Astron. Astrophys., 594 (2016), p. A13.
- [5] F. A. AHARONIAN ET AL., *Hitomi constraints on the 3.5 kev line in the perseus galaxy cluster*, ApJL, 837 (2017), p. L15.
- [6] Q. R. AHMAD ET AL., *Measurement of the rate of $\nu_e + d \rightarrow p + p + e^-$ interactions produced by ^8B solar neutrinos at the sudbury neutrino observatory*, Phys. Rev. Lett., 87 (2001), p. 071301.
- [7] E. K. AKHMEDOV, V. RUBAKOV, AND A. Y. SMIRNOV, *Baryogenesis via neutrino oscillations*, Phys. Rev. Lett., 81 (1998), p. 1359.
- [8] T. ASAKA AND M. SHAPOSHNIKOV, *The νmsm , dark matter and baryon asymmetry of the universe*, Phys. Lett. B, 620 (2005), pp. 17–26.
- [9] L. BAUDIS, *Dark matter searches*, Ann. Phys., 528 (2016), pp. 74–83.
- [10] A. BOYARSKY, O. RUCHAYSKIY, D. IAKUBOVSKIY, AND J. FRANSE, *Unidentified line in x-ray spectra of the andromeda galaxy and perseus galaxy cluster*, Phys. Rev. Lett., 113 (2014), p. 251301.
- [11] E. BULBUL, M. MARKEVITCH, A. FOSTER, R. K. SMITH, M. LOEWENSTEIN, AND S. W. RANDALL, *Detection of an unidentified emission line in the stacked x-ray spectrum of galaxy clusters*, Astroph. J., 789 (2014), p. 13.
- [12] J. CHADWICK, *The intensity distribution in the magnetic spectrum of β particles from radium*, Verhandl. Dtsc. Phys. Ges., 16 (1914), p. 383.
- [13] C. L. COWAN, F. REINES, F. B. HARRISON, H. W. KRUSE, AND A. D. MCGUIRE, *Detection of the free neutrino: a confirmation*, Science, 124 (1956), pp. 103–104.
- [14] A. R. CURTIS, *An eighth order runge-kutta process with eleven function evaluations per step*, Num. Math., 16 (1970), pp. 268–277.
- [15] S. DODELSON AND L. M. WIDROW, *Sterile neutrinos as dark matter*, Phys. Rev. Lett., 72 (1994), p. 17.

- [16] A. DOLGOV ET AL., *Cosmological bounds on neutrino degeneracy improved by flavor oscillations*, Nucl. Phys. B, 632 (2002), pp. 363–382.
- [17] A. FRIEDMAN, *On the curvature of space*, Z. Phys., 10 (1922), pp. 377–386.
- [18] Y. FUKUDA ET AL., *Evidence for oscillation of atmospheric neutrinos*, Phys. Rev. Lett., 81 (1998), pp. 1562–1567.
- [19] M. FUKUGITA AND T. YANAGIDA, *Barygenesis without grand unification*, Phys. Lett. B, 174 (1986), pp. 45–47.
- [20] A. HARADA AND A. KAMADA, *Structure formation in a mixed dark matter model with decaying sterile neutrino: the 3.5 keV x-ray line and the galactic substructure*, J. Cosmol. Astropart. Phys., 2016 (2016), p. 031.
- [21] J. HIDAKA AND G. M. FULLER, *Sterile neutrino-enhanced supernova explosions*, Phys. Rev. D, 76 (2007), p. 083516.
- [22] E. HUBBLE, *A relation between distance and radial velocity among extra-galactic nebulae*, Proc. Natl. Acad. Sci., 15 (1929), pp. 168–173.
- [23] Y. I. IZOTOV, T. X. THUAN, AND V. A. LIPOVETSKY, *The primordial helium abundance from a new sample of metal-deficient blue compact galaxies*, Astrophys. J., 435 (1994), pp. 647–667.
- [24] C. T. KISHIMOTO AND G. M. FULLER, *Lepton-number-driven sterile neutrino production in the early universe*, Phys. Rev. D, 78 (2008), p. 023524.
- [25] M. R. LOVELL, C. S. FRENK, V. R. EKE, A. JENKINS, L. GAO, AND T. THEUNS, *The properties of warm dark matter haloes*, Mon. Not. R. Astron. Soc., (2014), p. stt2431.
- [26] U. MAIO AND M. VIEL, *The first billion years of a warm dark matter universe*, Mon. Not. R. Astron. Soc., 446 (2015), pp. 2760–2775.
- [27] B. H. MCKELLAR AND M. J. THOMSON, *Oscillating neutrinos in the early universe*, Phys. Rev. D, 49 (1994), p. 2710.
- [28] S. MIKHEEV AND A. Y. SMIRNOV, *Resonance enhancement of oscillations in matter and solar neutrino spectroscopy*, Sov. J. Nucl. Phys.(Engl. Transl.);(United States), 42 (1985).
- [29] W. PAULI, *Letter to the radioactives in tübingen, december 1930, reproduced in cambridge monogr*, Part. Phys. Nucl. Phys. Cosmol, 14 (2000).
- [30] B. PONTECORVO, *Mesonium and anti-mesonium*, Sov. Phys. JETP, 6 (1957), p. 429.
- [31] L. STODOLSKY, *Treatment of neutrino oscillations in a thermal environment*, Phys. Rev. D, 36 (1987), pp. 2273–2277.
- [32] T. VENUMADHAV, F.-Y. CYR-RACINE, K. N. ABAZAJIAN, AND C. M. HIRATA, *Sterile neutrino dark matter: Weak interactions in the strong coupling epoch*, Phys. Rev. D, 94 (2016), p. 043515.
- [33] Z. XING AND S. ZHOU, *Neutrinos in Particle Physics, Astronomy and Cosmology*, Springer Science & Business Media, Zhejiang University Press, Hangzhou, China, 2011.